Master's thesis

NTNU
Norwegian University of Science and Technology
Faculty of Natural Sciences
Department of Physics

Christian Svingen Johnsen

Elements of the Microscopic Origins of Time-Reversal Symmetry Breaking in Phase-Frustrated Multiband Superconductors

Master's thesis in Applied Physics and Mathematics
Supervisor: Professor Asle Sudbø
June 2021

NTNU
Norwegian University of
Science and Technology

Christian Svingen Johnsen

Elements of the Microscopic Origins of Time-Reversal Symmetry Breaking in Phase-Frustrated Multiband Superconductors

Master's thesis in Applied Physics and Mathematics
Supervisor: Professor Asle Sudbø
June 2021

Norwegian University of Science and Technology
Faculty of Natural Sciences
Department of Physics

NTNU
Norwegian University of
Science and Technology

Abstract

Following the discovery of multiband superconductivity in the class of materials knows as iron pnictides, a series of theoretical and experimental studies have been published. Motivated by these discoveries and seeking to expand the theoretical understanding of the iron pnictides, we investigate a superconductor with three bands crossing the Fermi surface using mean-field theory. In this thesis, special emphasis is placed on understanding the microscopic origins of phase frustration arising with competing Josephson couplings internal to the superconductor because phase-frustrated superconductors can in some cases enter quantum states which break time-reversal symmetry and have spontaneous local magnetism. By deriving the generalized gap equations and free energy, we find that it is crucial to have three or more bands and that certain conditions must be met by the Josephson couplings and intraband potentials for there to be phase frustration. Some general combinations of microscopic parameters are shown to be able to lead to time-reversal symmetry breaking, and an analytical expression explaining some previous phenomenologically derived results is derived before performing numerical calculations. We find some numerical results regarding the onset of time-reversal symmetry breaking which are similar to previous studies, now through varying microscopic parameters and solving the gap equations directly. Finally, we model tuning the chemical potential, making the superconductor go from two to three bands and a time-reversal symmetry breaking state, thus giving a demonstration of how the densities of states at the Fermi surface and having three or more bands are key to the novel superconducting states in the iron pnictides.

Sammendrag

En rekke teoretiske og eksperimentelle studier har blitt publisert som følge av oppdagelsen av superledning i materialene ved navn jernpniktider. Med disse oppdagelsene som motivasjon og et mål om å utvide den teoretiske forståelsen av jernpniktidene undersøker vi en superleder med tre energibånd som krysser Fermiflaten på middelfeltnivå. På grunn av muligheten for kvantetilstander som bryter tidsinversjonssymmetri og for spontant genererte lokale magnetfelt legger vi i denne oppgaven spesiell vekt på å forstå det mikroskopiske opphavet til fasefrustrasjon forårsaket av konkurrerende interne Josephsonkoblinger i superledere. Ved å utlede generaliserte gapligninger og fri energi demonstrerer vi at tre eller flere energibånd i tillegg til visse vilkår for Josephsonkoblingskonstantene og intrabåndpotensialene er nødvendige for å få fasefrustrasjon. Vi viser så at enkelte generelle kombinasjoner av de mikroskopiske teoriparametrene kan føre til tidsinversjonssymmetribrudd og et analytisk uttrykk som forklarer et tidligere fenomenologisk utledet resultat vises før vi går videre til numeriske beregninger. Vi presenterer noen resultater rundt når en får tidsinversjonssymmetribrudd. Disse ligner andre studiers resultater, men denne gangen finnes de ved å variere mikroskopiske parametre og gjennom å løse gapligningene direkte. Til slutt modellerer vi hvordan en ved å øke det kjemiske potensialet kan få en superleder til å gå fra to bånd uten fasefrustrasjon til tre bånd og en tidsinversjonssymmetrybrytende tilstand og viser derved hvordan tilstandstettheten ved Fermiflaten og det å ha mer enn to bånd spiller nøkkelroller i de nye superledende tilstandene observert i jernpniktider.

Preface

This master's thesis was written during my tenth and final semester of the study program Applied Physics and Mathematics at the Norwegian University of Science and Technology. Some of the work leading up to the theory part of the thesis was performed in the latter part of 2020 in connection with a smaller project thesis I wrote that semester, but I wrote most of the thesis and the thousands of lines of code producing the results herein between the months of January and June in 2021.

Throughout the past year I have received plenty of help, advice and sagacious suggestions from my supervisor, Professor Asle Sudbø. I express my warmest thanks to him for his infectious enthusiasm and invaluable guidance. My dear family has also been there for me during all my five years here, and I thank them for never stopping believing in me and always encouraging me to keep going. I would also like to thank my friends who helped keep me somewhat sane through these arduous months of thesis work, giving special thanks to my good friend Niels Henrik for useful discussions and asking "stupid questions" which, in fact, are not always so stupid.

Christian Svingen Johnsen
Trondheim, Norway
June 25$^{\text{th}}$, 2021

Contents

Chapter 1

Introduction

1.1 Background and motivation

Due to its current and future enticing technological applications and richness in new physics to explore, superconductivity attracts wide interest from scientists and laypeople alike. The research field has roots going all the way back to the beginning of the last century, essentially to Onnes et al.'s 1911 discovery that mercury exhibited a precipitous drop in DC resistance when cooled down to below the critical temperature of $T_c \approx 4\,\mathrm{K}$ [1]. It would later become clear that in addition to becoming a perfect conductor, there was another characteristic behavior of superconductors: the expulsion of magnetic field lines from all of the superconductor except for a thin outer layer. This phenomenon, which only occurs for magnetic field strengths below a certain threshold, has been named the Meissner effect and was discovered by Meissner and Ochsenfeld in 1933 [2].

On the theory side of things, the community soon began the search for physical explanations of how superconductivity comes about, but it would still take another few decades of research for a first-principles explanation of the origins of superconductivity to emerge. As an example of one of the theoretical developments made before the much-celebrated microscopic theory of Bardeen, Cooper, and Schrieffer, we mention Ginzburg-Landau theory (GL theory). Published in 1950, the theory took a semi-phenomenological approach to the description of electromagnetic properties of superconductors near T_c and remains to this day a useful tool for such descriptions, sometimes by means of minor modifications of the original theory [3]. The authors took inspiration from Landau theory where there is some ordering present below a certain critical temperature and postulated an expression for the free energy density of a superconductor [4]. The energy involves the superconducting wavefunction ψ – which in modern language has the property that $|\psi|^2$ is the density of Cooper pairs – as well as the magnetic flux density $\mathbf{B} = \boldsymbol{\nabla} \times \mathbf{A}$, the magnetic vector potential $\mathbf{A}$, and the coupling between these quantities. By minimizing this energy, one can derive the first and second Ginzburg-Landau equation, the latter of which predicts the existence of a *supercurrent*, a frictionless flow of electrons coming from the spatial gradient of ψ's complex phase and $\mathbf{A}$. Additionally, GL theory predicts the existence of the Meissner effect [5].

Although GL theory is useful and captures some of the properties of superconductors, it does not capture all of them, nor does it attempt to explain superconductivity microscopically. For example, one property left unexplained in 1950s was the *isotope effect* which is the fact that increasing the mass M of the specific isotope comprising the atomic lattice decreases the critical temperature [6, 7]. These experiments suggested that interactions with the lattice were of importance in the mechanism behind superconductivity, and in 1957, the famous BCS theory was finally published [8]. The authors had envisaged pairs of electrons called Cooper pairs attracting each other via quantized lattice vibrations, or *phonons*, and found that their theory could describe many of the main features of superconductivity known at the time, including the isotope effect.

BCS remained a successful microscopic theory of superconductivity for a long time, even though a

slight modification of it appeared in 1959 when Suhl, Matthias, and Walker considered scattering of pairs of electrons between different energy bands crossing the Fermi surface [9]. Within each energy band, though, electrons could still attract each other pairwise like in the original BCS theory. This multiband theory remained a theoretical prediction until two-band [10, 11] superconductivity [12] was detected in MgB_2 with $T_c \approx 39\,\mathrm{K}$ two decades ago. At this point, the theory's predictions of a common T_c for the two gaps when interband scattering was present and the gaps' temperature dependence were compared to experiment, and these turned out to be in reasonable agreement. However, one detail not explicitly treated in the theory is the fact that in some cases, there can be a phase difference of π between the two gaps, i.e. one gap can have a negative sign [13–15].

This line of thought was pursued further, and researchers began investigating a Josephson junction consisting of a two-band superconductor and a single-band superconductor at the theoretical level [13, 14]. It quickly became clear that the phase difference could be subject to phase fluctuations [16, 17] or simply be different from π and 0 to minimize the energy of the $2+1$-band superconductor, implying that the gaps were complex numbers which could not be taken to be signed real numbers. This brings us closer to the main motivation of this thesis, as superconductors with three complex order parameters with phase differences not equal to π or 0 are predicted to display time-reversal symmetry breaking (TRSB) and local spontaneous magnetic fields [18, 19]. If found, such materials would therefore exhibit qualitatively new superconducting behavior. As we will see, this is indeed the case.

About a decade ago, the discovery of superconductivity at high T_c in iron pnictide materials sparked renewed excitement for the field of multiband superconductivity [20, 21]. This first discovery was in $LaO_{1-x}F_xFeAs$ with $T_c \approx 26\,\mathrm{K}$ at optimal doping $x \approx 0.11$. Another iron pnictide superconductor is the substance $Ba_{1-x}K_xFe_2As_2$ which has at least four superconducting gaps and $T_c = 38\,\mathrm{K}$ at doping level $x \approx 0.4$ [22, 23]. In a 2020 article, spontaneous magnetic fields and a TRSB state in this compound were reported for doping levels $0.7 \lesssim x \lesssim 0.85$ when $T \lesssim 10\,\mathrm{K}$ using the muon spin relaxation technique and data from the literature [24]. There is therefore already ample evidence that iron pnictide compounds in which more than two bands cross the Fermi surface display novel superconducting states [21–24].

Let us now look at some of theoretical developments that took place after the 2008 discoveries, many of which were at a semi-phenomenological level or . One early development was the work of Ng and Nagaosa [25]. They studied a two-band superconductor in a Josephson junction with a one-band superconductor using GL theory and found a TRSB state with a phase difference which was not a multiple of π. They also noted that this lead to a Josephson current circulating in momentum space.

Later, Stanev and Tešanović followed Ng and Nagaosa's suggestion of studying a three-band superconductor where the Josephson couplings are all between bands *internal* to the same superconductor [26]. The authors used a three-band version of the generalized BCS Hamiltonian suggested in [9] in the mean-field approximation. They sought to understand the model by considering three equal bands and only allowing interband couplings, two of which were equal. By linearizing the BCS-like gap equations near T_c, Stanev and Tešanović found three sets of solutions, two of which they linearly combined with complex coefficients to create a solution with two non-real superconducting gaps and one real. The two remaining solutions were one with only two gaps and one with three real gaps. After having identified different possible structures of the gaps, parametrizations of these were put into the gap equations, this time expanded to second order in the gap magnitudes. The results were that the complex, TRSB solution had the lowest free energy in GL theory – and was therefore the state the system would choose – in a small range of interband couplings near the point where they were equal. The existence of a TRSB solution with no intraband couplings for interband couplings of the same magnitude but various sign combinations was also reported by Tanaka and Yanagisawa, this time obtained directly from BCS-like gap equations with explicitly complex gaps [27].

Maiti and Chubukov performed an analysis similar to the ones above, but with a focus on modeling hole doping in $Ba_{1-x}K_xFe_2As_2$ by varying interband couplings [28]. A similar phase diagram was found, but they noted that the disappearance of the third gap was a peculiarity of the minimal model they studied.

After these (mostly) mean-field calculations, some numerical calculations and Monte Carlo simula-

tions have also been performed to investigate the effects of different types of fluctuations [29–32]. In 2013, for example, Bojesen, Babaev, and Sudbø investigated, at a phenomenological level, a three-band superconductor using *short time critical dynamics*, finding in some cases different temperature onsets of superconductivity and TRSB [31]. These calculations, however, did not attempt to capture microscopic details and took the interband Josephson coupling strengths multiplied by the gap amplitudes $|\psi|$ in the GL theory as fundamental. In one calculation, two of these couplings were held constant while the third was increased gradually, which revealed that TRSB did not occur until the third coupling was at least half as large as the others. For some values of the phenomenological interband couplings and temperatures, the TRSB state was metallic, i.e. not superconducting. In 2015, again using Monte Carlo methods, Bojesen and Sudbø showed that going beyond mean-field theory and including gauge field fluctuations was necessary to produce a TRSB metallic state [32].

With these theoretical results in mind, we can now articulate the motivation behind this thesis. Many previous studies either phenomenologically or using restrictive assumptions have investigated three-band superconductors at different levels of detail. We wish to study a three-band superconductor with internal Josephson couplings as a simplified example of the iron pnictides, seeking to understand microscopically and by directly using the BCS-like multi-gap equations, with fewer assumptions than previous studies, how the fascinating superconducting states which break time-reversal symmetry come about.

Some of the interest in these materials is rooted in the aforementioned fact that time-reversal symmetry breaking states can have intrinsic magnetism [19, 18] which we in principle could turn on and off by moving the Fermi surface up or down in energy so as to change the number of bands crossing it. This tuning of μ can be done by e.g. doping [24] or more directly by applying an electric field to deform the Fermi surface [33]. There may therefore even be possible technological applications of these novel compounds in the future. Applications may of course also come as a second-order effect from increased understanding of high-T_c mechanisms in superconductors, which is another possibility seeing as some iron pnictides display rather high critical temperatures.

Chapter 2

Preliminaries

2.1 Conventions

We will use natural units, $\hbar = 1 = k_{\mathrm{B}}$ and make no special symbolical distinction between operators and numbers.

2.2 Bardeen–Cooper–Schrieffer theory of superconductivity

The microscopic theory of superconductivity proposed by BCS is formulated as a Hamiltonian

$$H = H_{\mathrm{kin}} + H_{\mathrm{int}}, \tag{2.1}$$

a function of operators, particle excitation energies, and particle interactions from which one can calculate thermodynamic properties of interest [34]. We will in this subsection construct the BCS Hamiltonian step by step, starting with the kinetic term H_{kin} which, on its own, describes free electrons which are essentially only constrained by the Pauli principle.

Using the language of *second quantization* [35], then, we can model a gas of such non-interacting electrons using only the Hamiltonian H_{kin} which will consist of creation and destruction operators $c^\dagger_{\mathbf{k}\sigma}$, $c_{\mathbf{k}\sigma}$ that either create or destroy a state of one electron with spin σ and linear momentum $\mathbf{k}$. The operator $c^\dagger_{\mathbf{k}\sigma}$, which is known as the *adjoint* or *Hermitian conjugate* of $c_{\mathbf{k}\sigma}$, creates the plane wave state $(\mathbf{k}, \sigma)$ whereas $c_{\mathbf{k}\sigma}$ destroys it. The electron this state represents has an excitation energy $\varepsilon_{\mathbf{k}\sigma}$ which we later in the thesis will assume to have a simple spin-independent and parabolic form, but for now we leave it unspecified. Electrons are fermions, so they obey the Pauli principle, meaning at most *one* electron can occupy any single-particle quantum state $(\mathbf{k}, \sigma)$. This fact is encapsulated by the fermionic *anticommutation* relations

$$\left\{c^\dagger_{\mathbf{k}\sigma}, c_{\mathbf{k}'\sigma'}\right\} \equiv c^\dagger_{\mathbf{k}\sigma} c_{\mathbf{k}'\sigma'} + c_{\mathbf{k}'\sigma'} c^\dagger_{\mathbf{k}\sigma} = \delta_{\mathbf{k}\mathbf{k}'}\delta_{\sigma\sigma'}, \tag{2.2}$$

which we will assume hold for our creation and destruction operators. In this equation, the symbols on the right-hand side are Kronecker deltas which have the property that $\delta_{\mu\nu} = 1$ if $\mu = \nu$ and are zero otherwise. Furthermore, we have that the anticommutators

$$\{c_{\mathbf{k}\sigma}, c_{\mathbf{k}'\sigma'}\} = \left\{c^\dagger_{\mathbf{k}\sigma}, c^\dagger_{\mathbf{k}'\sigma'}\right\} = 0. \tag{2.3}$$

The final ingredient necessary to specify the free electron Hamiltonian H_{kin} is the number operator $n_{\mathbf{k}\sigma} = c^\dagger_{\mathbf{k}\sigma} c_{\mathbf{k}\sigma}$, an operator which counts how many electrons are in the state $(\mathbf{k}, \sigma)$. Now, the Hamiltonian is simply the sum of the excitation energies of all the electrons in the system:

$$H_{\mathrm{kin}} = \sum_{\mathbf{k},\sigma} \varepsilon_{\mathbf{k}\sigma} c^\dagger_{\mathbf{k}\sigma} c_{\mathbf{k}\sigma}. \tag{2.4}$$

Here, the number operator multiplying each excitation energy in the sum over all the possible single-particle states $(\mathbf{k}, \sigma)$ makes sure only the energies of states that are *occupied* are counted.

So far, we are only considering electrons floating around in a vacuum without being affected by each other. In real-world materials, and certainly in iron pnictides and metals that can become superconducting, there are also positively charged atomic nuclei which comprise a lattice in addition to the electrons in the materials' atoms. We will need to include these facts in the interaction Hamiltonian, H_{int}, in order to have at least a reasonable description of the materials in line with experimental evidence. The electrons moving around on the lattice are close enough that their interactions with each other cannot simply be ignored out of hand, and furthermore, because of the hint from the isotope effect, one should include interactions $V_{e^- - \text{ph}}$ between electrons and phonons, i.e. include interactions where electrons scatter off the lattice nuclei and cause them to vibrate "quantum mechanically". The Hamiltonian of such a system would be

$$H = H_{\text{kin}} + \sum_{\mathbf{k},\mathbf{k}',\mathbf{q},\sigma,\sigma'} \frac{1}{4\pi\varepsilon_0} \frac{2\pi e^2}{\mathbf{q}^2} c^\dagger_{\mathbf{k}+\mathbf{q},\sigma} c^\dagger_{\mathbf{k}'-\mathbf{q},\sigma'} c_{\mathbf{k}\sigma} c_{\mathbf{k}'\sigma'} + V_{e^- - \text{ph}}, \tag{2.5}$$

but for our purposes it suffices to combine two such electron-phonon interactions into an *effective interaction* $V_{\text{eff}}(\mathbf{k}, \mathbf{k}', \mathbf{q})$, essentially hiding some of the details of the phonons and just keeping the fact that there is another way for electrons to interact besides via photons [5]. We can therefore write

$$H = H_{\text{kin}} + \sum_{\mathbf{k},\mathbf{k}',\mathbf{q},\sigma,\sigma'} \tilde{V}_{\text{eff}}(\mathbf{q}, \omega) c^\dagger_{\mathbf{k}+\mathbf{q},\sigma} c^\dagger_{\mathbf{k}'-\mathbf{q},\sigma'} c_{\mathbf{k}\sigma} c_{\mathbf{k}'\sigma'} \tag{2.6}$$

where the energy transfer is

$$\omega = \varepsilon_{\mathbf{k}+\mathbf{q}} - \varepsilon_{\mathbf{k}}, \tag{2.7}$$

and the effective interaction including both photon- and phonon-mediated electron-electron interactions has the form

$$\tilde{V}_{\text{eff}}(\mathbf{q}, \omega) = 2|M_{\mathbf{q}}|^2 \frac{\omega_{\mathbf{q}}}{\omega^2 - \omega^2_{\mathbf{q}}} + \frac{1}{4\pi\varepsilon_0} \frac{2\pi e^2}{\mathbf{q}^2}. \tag{2.8}$$

Here, $M_{\mathbf{q}}$ is the matrix element for the electron-phonon coupling. It contains the atomic mass and could be used to calculate the isotope effect. We will, however, not keep such details moving forward as we would like to end up with a theory that does not specifically require phonons to mediate the interactions. In fact, the only detail we will keep is that there is some attraction between electrons.

Where would such an attraction come from? The effective interaction, $\tilde{V}_{\text{eff}}(\mathbf{q}, \omega)$, has two small intervals along the ω axis where it it is negative, i.e. *attractive*. It can even take on arbitrarily large negative values as ω approaches $\omega_{\mathbf{q}}$ from below, meaning it can overcome the static repulsion term as long as ω gets close enough to $\omega_{\mathbf{q}}$.

2.3 Generalized BCS theory of superconductivity

In this section, we will simplify the Hamiltonian under consideration, keeping only the essential ingredient necessary for there to be superconductivity, namely a sufficiently strong *attraction* between electrons with certain momenta. We will also extend the model to N bands crossing the Fermi surface in the spirit of [9] before applying a mean-field approximation analogously to what is normally done in BCS theory.

The effective potential $\tilde{V}_{\text{eff}}(\mathbf{q}, \omega)$ is in reality only attractive for specific ω^2 near $\omega^2_{\mathbf{q}}$ as noted, but it turns out that to get both quantitatively and qualitatively correct predictions from the model, it suffices to retain only one feature of $\tilde{V}_{\text{eff}}(\mathbf{q}, \omega)$, namely that it is attractive for certain ω [5]. We will therefore extend the set of ω's for which $\tilde{V}_{\text{eff}}(\mathbf{q}, \omega)$ is attractive from the two sets of ω where ω^2 is near but slightly smaller than $\omega_{\mathbf{q}}$ to the entire interval $[-\omega_{\mathbf{q}}, \omega_{\mathbf{q}}]$. Moreover, we remove any other ω-dependence by setting the potential to be constantly zero for $\omega^2 > \omega^2_{\mathbf{q}}$, leaving us with a simple square well of width $2\omega_{\mathbf{q}}$ centered at $\omega = 0$. It is with this final, dramatic simplification that we say we only keep the fact that there is an attraction between electrons; almost all details of phonons and photons are hidden. We now follow BCS

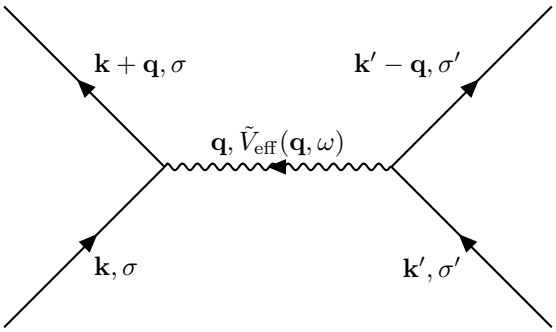

Figure 2.1: Momentum-space Feynman diagram of an envisaged effective two-particle interaction that can be attractive for certain momenta and energy transfers. With time increasing upwards, this diagram represents a pair of electrons $(\mathbf{k},\sigma)$, $(\mathbf{k}',\sigma')$ interacting via an effective potential $V_{\text{eff}}(\mathbf{k},\mathbf{k}',\mathbf{q})$ which represents, in a simplified way, the screened Coulomb repulsion *and* the exchange of another boson (e.g. a phonon), with total momentum transfer $\mathbf{q}$ and energy transfer ω.

[8] and assume that the energy range $2\omega_{\mathbf{q}}$ is exceedingly small compared to the Fermi energy. This implies that we have scattering between slightly different energy states, which, due to the Pauli principle, will have to take place near the Fermi surface which is the only place in momentum space that has occupied and unoccupied single-particle states in close vicinity when we are close to the ground state. To further simplify and consider only the most pairing-friendly pairs of electrons, we consider *spin-singlet pairing*, i.e. $\sigma = -\sigma'$. The geometry of this problem now dictates that for most $\mathbf{q}$, the easiest way to have both $\mathbf{k}+\mathbf{q}$ and $\mathbf{k}'-\mathbf{q}$ in the thin area around the Fermi surface is to have $\mathbf{k}' = -\mathbf{k}$. Thus,

$$H = H_{\text{kin}} + \sum_{\mathbf{k},\mathbf{q},\sigma} \tilde{V}_{\text{eff}}(\mathbf{q},\omega) c^\dagger_{\mathbf{k}+\mathbf{q},\sigma} c^\dagger_{-\mathbf{k}-\mathbf{q},-\sigma} c_{\mathbf{k},\sigma} c_{-\mathbf{k},-\sigma} \tag{2.9}$$

If we let $\mathbf{k} \to \mathbf{k}-\mathbf{q}$ and $\mathbf{q} \to \mathbf{q}+\mathbf{k}$, we can relabel $\mathbf{q}$ and finally write

$$H = \sum_{\mathbf{k},\sigma} \varepsilon_{\mathbf{k}\sigma} c^\dagger_{\mathbf{k}\sigma} c_{\mathbf{k}\sigma} + \sum_{\mathbf{k},\mathbf{k}'} \tilde{V}_{\text{eff}}(\mathbf{k},\mathbf{k}',\omega) c^\dagger_{\mathbf{k}\uparrow} c^\dagger_{-\mathbf{k}\downarrow} c_{-\mathbf{k}'\downarrow} c_{\mathbf{k}'\uparrow} \tag{2.10}$$

having absorbed a factor two from the spin summation into the new effective potential $\tilde{V}_{\text{eff}}(\mathbf{k},\mathbf{k}',\omega)$.

We will now simplify some of the notation and change sign convention for the interaction potentials. First, when restricting ourselves to electrons near the Fermi surface $\varepsilon_{\text{F}} = \mu$, we must ensure that the initial and final states differ in energy by no more than some cut-off energy ω_{c}, which can be done by considering only initial and final momenta

$$\mathbf{k},\mathbf{k}' \in F \equiv \{\mathbf{k}'' \mid |\varepsilon_{\mathbf{k}''} - \mu| \leq \omega_{\text{c}}\}\,. \tag{2.11}$$

In the rest of the thesis, we will choose the other sign convention for the two-particle terms and use the potential

$$V(\mathbf{k},\mathbf{k}') = \begin{cases} -\tilde{V}_{\text{eff}}(\mathbf{k},\mathbf{k}',\omega) & \text{if both } \mathbf{k},\mathbf{k}' \in F \\ 0 & \text{otherwise} \end{cases}, \tag{2.12}$$

where a positive value means it is attractive and a negative one means it is repulsive. To arrive at the celebrated BCS gap equation, one would here apply a mean-field approximation and diagonalize the Hamiltonian. We will instead extend the theory to N energy bands crossing the Fermi surface and pair tunneling between bands before studying the Hamiltonian in the mean-field approximation.

2.3.1 Extension to multiple bands crossing the Fermi surface

The reduced Hamiltonian in the previous section can be extended to include electrons pairing in *multiple* bands by performing a summation over Hamiltonians H_α equivalent to the previous one,

$$H_\alpha = \sum_{\mathbf{k},\sigma} \varepsilon_{\mathbf{k}\sigma\alpha} c^\dagger_{\mathbf{k}\sigma\alpha} c_{\mathbf{k}\sigma\alpha} - \sum_{\mathbf{k},\mathbf{k}'} V_{\alpha,\alpha}(\mathbf{k},\mathbf{k}') c^\dagger_{\mathbf{k}\uparrow\alpha} c^\dagger_{-\mathbf{k}\downarrow\alpha} c_{-\mathbf{k}'\downarrow\alpha} c_{\mathbf{k}'\uparrow\alpha}, \tag{2.13}$$

where $\alpha = 1, \ldots, N$ is the band index. All the symbols in Eq. (2.13) have the same meaning as before, only with the added meaning of referring to energy band α. For instance, $c^\dagger_{\mathbf{k}\sigma\alpha}$ creates an electron in the state $(\mathbf{k},\sigma)$ in energy band α with excitation energy $\varepsilon_{\mathbf{k}\sigma\alpha}$. The sum of these Hamiltonians would result in N superconducting gaps, given that all *intraband* interactions

$$V_{\alpha,\alpha}(\mathbf{k},\mathbf{k}') = \begin{cases} V_{\alpha,\alpha} & \text{if both } \mathbf{k},\mathbf{k}' \in F_\alpha \\ 0 & \text{otherwise} \end{cases} \tag{2.14}$$

allow superconductivity. Also here, the constants $V_{\alpha,\alpha}$ – which are positive when attractive – originate with an effective potential $-\tilde{V}_{\text{eff}}(\mathbf{k},\mathbf{k}',\omega)$ associated with each band α, and F_α is, as in Eq. (2.11), the set of all momenta $\mathbf{k}$ in a thin shell around the Fermi surface where $|\varepsilon_{\mathbf{k}\sigma\alpha} - \mu|$ is no larger than the energy cutoff ω_α in band α. This summation over Hamiltonians, however, is just N decoupled superconductor Hamiltonians, meaning each Hamiltonian can be treated independently. The physics of interest, such as phase frustration and TRSB states, arises only when we consider, in addition to $\sum_\alpha H_\alpha$, terms $H_{\alpha\beta}$ describing scattering of electron pairs from the energy band labeled β to band α. Such terms involve the creation of two electrons in energy band α and their destruction in band β, and we simply denote the matrix element for this scattering process

$$V_{\alpha\beta}(\mathbf{k},\mathbf{k}') = \begin{cases} V_{\alpha\beta} & \text{if } \mathbf{k} \in F_\alpha \text{ and } \mathbf{k}' \in F_\beta \\ 0 & \text{otherwise} \end{cases}, \tag{2.15}$$

such that

$$H_{\alpha\beta} = -\sum_{\mathbf{k},\mathbf{k}'} V_{\alpha\beta}(\mathbf{k},\mathbf{k}') c^\dagger_{\mathbf{k}\uparrow\alpha} c^\dagger_{-\mathbf{k}\downarrow\alpha} c_{-\mathbf{k}'\downarrow\beta} c_{\mathbf{k}'\uparrow\beta}. \tag{2.16}$$

Adding all the H_α terms to the scattering terms $H_{\alpha\beta}$ (including the reverse process, $H_{\beta\alpha}$) and subtracting $\sum_{\mathbf{k}\sigma\alpha} \mu n_{\mathbf{k}\sigma\alpha}$ from H to measure energies relative to the chemical potential μ, we arrive at the N-band Hamiltonian which will be considered using a mean-field approximation in this thesis, namely

$$H = \sum_{\mathbf{k},\sigma,\alpha} \tilde{\varepsilon}_{\mathbf{k}\sigma\alpha} c^\dagger_{\mathbf{k}\sigma\alpha} c_{\mathbf{k}\sigma\alpha} - \sum_{\mathbf{k},\mathbf{k}',\alpha,\beta} V_{\alpha\beta}(\mathbf{k},\mathbf{k}') c^\dagger_{\mathbf{k}\uparrow\alpha} c^\dagger_{-\mathbf{k}\downarrow\alpha} c_{-\mathbf{k}'\downarrow\beta} c_{\mathbf{k}'\uparrow\beta}, \tag{2.17}$$

where the band indices α, β both take on the values $1, \ldots, N$ and $\tilde{\varepsilon}_{\mathbf{k}\sigma\alpha} = \varepsilon_{\mathbf{k}\sigma\alpha} - \mu$. We will eventually set $N = 3$ and $V_{\alpha\beta} = V_{\beta\alpha}$ in the Hamilonian so as to use the simplest possible model of e.g. the iron pnictides while still retaining the physics of interest.

The effective interactions we consider can all be represented neatly in a momentum-space Feynman diagram, as is done in Fig. 2.2. There, $\alpha = \beta$ represents two electrons moving in opposite directions near the Fermi surface attracting each other through the effective intraband interaction $V_{\alpha,\alpha}(\mathbf{k},\mathbf{k}')$, whereas $\alpha \neq \beta$ means the two electrons are scattered to a different energy band, again by an *effective* interaction, $V_{\alpha\beta}(\mathbf{k},\mathbf{k}')$. We will later assume, for simplicity, parabolic and spin-independent dispersion relations with different minimum energies for electrons in different bands, i.e.

$$\varepsilon_{\mathbf{k}\alpha} = \frac{\mathbf{k}^2}{2m} + \varepsilon_{0,\alpha}, \tag{2.18}$$

where $\varepsilon_{0,\alpha}$ is the minimum energy of band α and m is the electron mass. We will also order the minima $\varepsilon_{0,1} < \varepsilon_{0,2} < \varepsilon_{0,3}$ and set $N = 3$. This band structure is illustrated in two different ways in Fig. 2.3

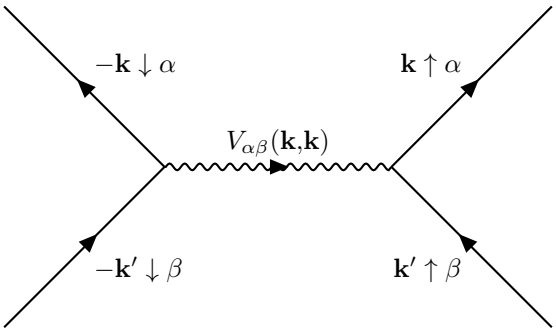

Figure 2.2: Momentum-space Feynman diagram of the various two-particle interactions considered in this thesis. With time increasing upwards, this diagram represents a pair of electrons $(\mathbf{k}',\uparrow)$, $(-\mathbf{k}',\downarrow)$ in orbital β interacting via some effective potential $V_{\alpha\beta}(\mathbf{k},\mathbf{k}')$. In conventional BCS theory, the wavy line representing the potential is a phonon propagator, but our model is agnostic to the underlying mechanism by which the electrons interact. The interband processes where $\alpha \neq \beta$ leaves the two oppositely moving electrons in another orbital, α, with new momenta $\mathbf{k}, -\mathbf{k}$ which are still oppositely directed. The intraband processes $\alpha = \beta$ are weak attractions, now leaving the pair in the same orbital after they interact. It was only this latter type of process that was considered in the original BCS theory of superconductivity.

for equal $\omega_\alpha \equiv \omega$ which are exaggerated in size for illustrative purposes. The excitation energies as a function of k_x at $k_y, k_z = 0$ are shown in Fig. 2.3a, including the thin energy shell of width 2ω around the Fermi level within which electrons must be to be affected by the interactions $V_{\alpha\beta}$. The energy shell is shown for two different values of μ as we will study the transition from $\mu = 0.6\mu_{\max}$ to $\mu_{\max}$ numerically in Chapter 4.3.2. The other figure, 2.3b, shows a slice through the energy shell $[\mu_{\max} - \omega, \mu_{\max} + \omega]$ in k_x, k_y-space at constant k_z in addition to example initial (red) and final (black) states of scattering from band 3 to 2.

2.3.2 Mean-field theory

The Hamiltonian in Eq. (2.17) cannot be exactly solved, but it can be simplified by using a mean-field approximation where fluctuations of the *Cooper pair operators* $c^\dagger_{\mathbf{k}\uparrow\alpha}c^\dagger_{-\mathbf{k}\downarrow\alpha}$ and $c_{-\mathbf{k}\downarrow\alpha}c_{\mathbf{k}\uparrow\alpha}$ are assumed to be small. Thereafter, the Hamiltonian can be diagonalized using a Bogoliubov transformation, yielding the energy spectrum of the long-lived quasiparticle excitations the Hamiltonian now describes [36].

The mean-field approximation we now employ is focused on the thermal averages,

$$\begin{aligned} b_{\mathbf{k}\alpha} &= \langle c_{-\mathbf{k}\downarrow\alpha}c_{\mathbf{k}\uparrow\alpha}\rangle \\ b^\dagger_{\mathbf{k}\alpha} &= \left\langle c^\dagger_{\mathbf{k}\uparrow\alpha}c^\dagger_{-\mathbf{k}\downarrow\alpha}\right\rangle, \end{aligned} \tag{2.19}$$

of Cooper pair destruction and creation operators. In general, the thermal average of an operator R is

$$\langle R\rangle = \frac{\sum_i \langle\psi_i|\, \mathrm{e}^{-\beta H} R\,|\psi_i\rangle}{\sum_i \langle\psi_i|\, \mathrm{e}^{-\beta H}\,|\psi_i\rangle}, \tag{2.20}$$

where $\{|\psi_i\rangle\}_i$ forms an orthonormal basis of the many-particle Fock space of the system under consideration and $\beta = 1/T$ is the inverse temperature [34]. We will not utilize this definition explicitly, but later we will make use of the denominator in Eq. (2.20) which is called the *partition function* Z of the system. Returning to the averages $b_{\mathbf{k}\alpha}, b^\dagger_{\mathbf{k}\alpha}$ in Eq. (2.19), we add and subtract these in all factors of

$$\begin{aligned} c_{-\mathbf{k}\downarrow\alpha}c_{\mathbf{k}\uparrow\alpha} &= b_{\mathbf{k}\alpha} + c_{-\mathbf{k}\downarrow\alpha}c_{\mathbf{k}\uparrow\alpha} - b_{\mathbf{k}\alpha} \equiv b_{\mathbf{k}\alpha} + \delta b_{\mathbf{k}\alpha}, \\ c^\dagger_{\mathbf{k}\uparrow\alpha}c^\dagger_{-\mathbf{k}\downarrow\alpha} &= b^\dagger_{\mathbf{k}\alpha} + c^\dagger_{\mathbf{k}\uparrow\alpha}c^\dagger_{-\mathbf{k}\downarrow\alpha} - b^\dagger_{\mathbf{k}\alpha} \equiv b^\dagger_{\mathbf{k}\alpha} + \delta b^\dagger_{\mathbf{k}\alpha} \end{aligned} \tag{2.21}$$

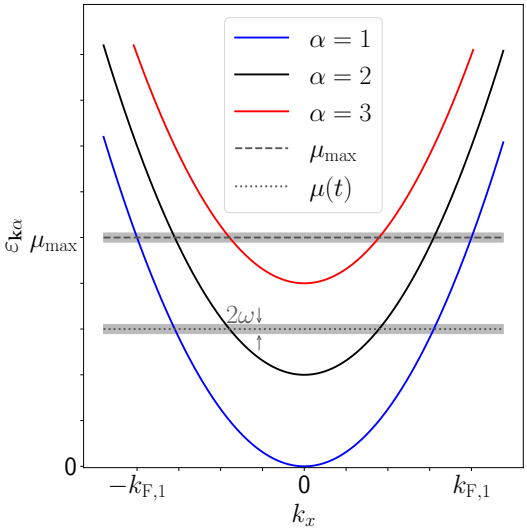

(a) An illustration of what the dispersion relations in our simplified three-band model look like for $k_y, k_z = 0$. The gray shaded area around the Fermi surface $\mu(t)$ represents the energy range within which the electrons are affected by the effective interactions. Here we simplify the thickness of the energy range to be the same value, 2ω, for all the bands, and make ω quite large for illustrative purposes. We will later see how tuning $\mu(t)$ from $0.6\mu_{\max}$ (bottom gray shaded area) to $\mu_{\max}$ can turn on time-reversal symmetry breaking if the interactions $V_{\alpha\beta}$ allow it.

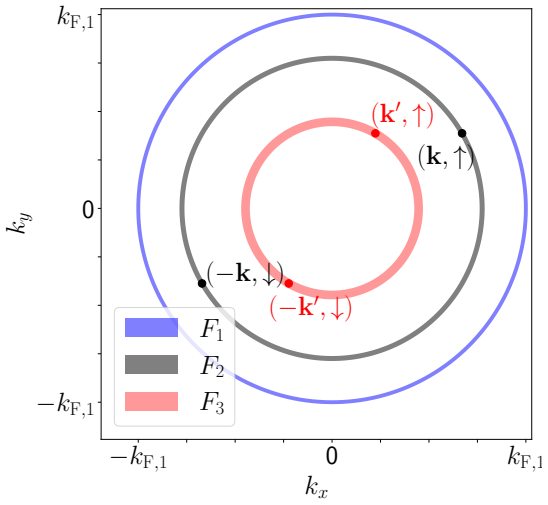

(b) An illustration of what the thin momentum shells F_α in our simplified three-band model look like in two out of three dimensions, given that the dispersion relations are as in Fig. 2.3a. This is essentially a slice through the uppermost gray shaded energy shell in Fig. 2.3a rotated around the energy axis. The two red dots in the red shaded area serve as an example of a possible initial state of an electron pair in energy band 3 before interacting through e.g. a phonon and ending up in the middle energy band, $\alpha = 2$. Such an end state may look like the two black dots in the gray shaded area.

Figure 2.3: Illustrations of the electronic structure of the three-band model we study in this thesis using mean-field theory.

in the Hamiltonian defined in Eq. (2.17) and ignore terms of second order in the fluctuation terms $\delta b_{\mathbf{k}\alpha}, \delta b^\dagger_{\mathbf{k}\alpha}$. Rearranging some of the sums, the Hamiltonian then reads

$$H \approx \sum_{\mathbf{k},\sigma,\alpha} \tilde{\varepsilon}_{\mathbf{k}\sigma\alpha} c^\dagger_{\mathbf{k}\sigma\alpha} c_{k\sigma\alpha} - \sum_{\mathbf{k},\mathbf{k}',\alpha,\beta} V_{\alpha\beta}(\mathbf{k},\mathbf{k}') \left(b^\dagger_{\mathbf{k}\alpha} c_{-\mathbf{k}'\downarrow\beta} c_{\mathbf{k}'\uparrow\beta} + \text{h.c.} - b^\dagger_{\mathbf{k}\alpha} b_{\mathbf{k}'\beta} \right), \tag{2.22}$$

which can be rewritten to contain the *superconducting gap functions* $\Delta_\alpha(\mathbf{k})$ which we are about to define.

We first label the sum over the last term in Eq. (2.22) $\tilde{E}_0$ and move the momentum-dependence of the potentials to the functions $\eta_\alpha(\mathbf{k})$ so as to have

$$V_{\alpha\beta}(\mathbf{k},\mathbf{k}') = \eta_\alpha(\mathbf{k})\eta_\beta(\mathbf{k}')V_{\alpha\beta} \tag{2.23}$$

and

$$H = H_{\text{kin}} + \tilde{E}_0 - \sum_{\mathbf{k},\mathbf{k}',\alpha,\beta} \eta_\alpha(\mathbf{k})\eta_\beta(\mathbf{k}')V_{\alpha\beta} \left(b^\dagger_{\mathbf{k}\alpha} c_{-\mathbf{k}'\downarrow\beta} c_{\mathbf{k}'\uparrow\beta} + \text{h.c.} \right). \tag{2.24}$$

In our case, with momentum-dependent potentials as defined in Eq. (2.15),

$$\eta_\alpha(\mathbf{k}) = \begin{cases} 1 & \text{if } \mathbf{k} \in F_\alpha \\ 0 & \text{otherwise} \end{cases}, \tag{2.25}$$

but we could in principle have left $\eta_\alpha(\mathbf{k})$ unspecified for the moment and used Eq. (2.23) as a separability ansatz for the potentials. The function multiplying the two annihilation operators in Eq. (2.24) for each $\mathbf{k}'$ and β is now

$$\sum_{\mathbf{k},\alpha} V_{\alpha\beta}\eta_\beta(\mathbf{k}')\eta_\alpha(\mathbf{k}) b^\dagger_{\mathbf{k}\alpha} = \eta_\beta(\mathbf{k}')(\mathbf{b}^\dagger \mathbf{V})_\beta \tag{2.26}$$

where we have defined the row vector $\mathbf{b}^\dagger$ with components

$$b^\dagger_\alpha = \sum_{\mathbf{k}} \eta_\alpha(\mathbf{k}) b^\dagger_{\mathbf{k}\alpha} = \sum_{\mathbf{k}\in F_\alpha} b^\dagger_{\mathbf{k}\alpha} \tag{2.27}$$

and the matrix $\mathbf{V}$ with entries $V_{\alpha\beta}$. A similar sum of $b_{\mathbf{k}\alpha}$ for momenta near the Fermi surface defines the column vector $\mathbf{b}_\alpha$ which is hidden in the h.c. term in the Hamiltonian. It is precisely the expression in Eq. (2.26) that is what we will refer to as the superconducting gap function:

$$\begin{aligned} \Delta_\alpha(\mathbf{k}) &\equiv \eta_\alpha(\mathbf{k})(\mathbf{V}\mathbf{b})_\alpha \;\; = \eta_\alpha(\mathbf{k}) \sum_\beta V_{\alpha\beta} b_\beta, \\ \Delta^\dagger_\alpha(\mathbf{k}) &\equiv \eta_\alpha(\mathbf{k})(\mathbf{b}^\dagger\mathbf{V})_\alpha = \eta_\alpha(\mathbf{k}) \sum_\beta V_{\alpha\beta} b^\dagger_\beta. \end{aligned} \tag{2.28}$$

Here, we make two remarks before writing down the Hamiltonian using the gap function and its complex conjugate $\Delta^\dagger_\alpha(\mathbf{k})$. Firstly, due to the factor $\eta_\alpha(\mathbf{k})$, gap function α completely vanishes if energy band $\varepsilon_{\mathbf{k}\alpha}$ does not overlap with the Fermi surface μ for any $\mathbf{k}$, i.e. if $\varepsilon_{0,\alpha} > \mu$.[1] Secondly, the N gap functions each contain a term $V_{\alpha\alpha}b_\alpha \propto \sum \langle c_{-\mathbf{k}\downarrow\alpha} c_{\mathbf{k}\uparrow\alpha} \rangle$ from their own energy band, α, but also terms $V_{\alpha\beta}b_\beta \propto \sum \langle c_{-\mathbf{k}\downarrow\beta} c_{\mathbf{k}\uparrow\beta} \rangle$, i.e. contributions from *other* energy bands given that $V_{\alpha\beta} \neq 0$. The latter terms are a consequence of the fact that the Hamiltonian we started out with in Eq. (2.17) described N *coupled* superconductors. Now, however, the coupling of the problem has been relegated to the definition of the gaps because the Hamiltonian,

$$H = H_{\text{kin}} + \tilde{E}_0 - \sum_{\mathbf{k},\alpha} \left(\Delta^\dagger_\alpha(\mathbf{k}) c_{-\mathbf{k}\downarrow\alpha} c_{\mathbf{k}\uparrow\alpha} + \Delta_\alpha(\mathbf{k}) c^\dagger_{\mathbf{k}\uparrow\alpha} c^\dagger_{-\mathbf{k}\downarrow\alpha} \right), \tag{2.29}$$

[1] Strictly speaking, $\Delta_\alpha(\mathbf{k})$ vanishes if $\varepsilon_{0,\alpha} > \mu + \omega_\alpha$, but the assumption here is that ω_α is negligible compared to μ. Again, this situation is illustrated in Fig. 2.3a where the lower of the two gray areas only crosses two of the bands.

is diagonal in the band indices. Here, we see that $\Delta_\alpha(\mathbf{k})$ acts like the strength of a source of Cooper pairs of electrons with momentum $\pm\mathbf{k}$ in band α, whereas $\Delta_\alpha^\dagger(\mathbf{k})$ is the strength of a sink of such pairs. As a final note, we observe that the Hamiltonian can be rewritten to

$$H = H_{\text{kin}} + \tilde{E}_0 - \sum_\alpha \sum_{\mathbf{k}\in F_\alpha} \left(\Delta_\alpha^\dagger c_{-\mathbf{k}\downarrow\alpha} c_{\mathbf{k}\uparrow\alpha} + \Delta_\alpha c_{\mathbf{k}\uparrow\alpha}^\dagger c_{-\mathbf{k}\downarrow\alpha}^\dagger \right) \tag{2.30}$$

by defining momentum-independent gaps Δ_α exactly like in Eq. (2.28) except without the factors $\eta_\alpha(\mathbf{k})$. These are the gap functions we will refer to and calculate numerically, although sometimes it will be convenient to reinstate the $\mathbf{k}$-dependence of the gaps for certain calculations. Before showing the properly generalized Bogoliubov transformation that allows us to diagonalize the above Hamiltonian while preserving the gaps' complex phases, we need to introduce two key concepts.

2.4 Frustration and time-reversal symmetry breaking

As will be shown soon, $N \geq 3$-band superconductors can experience frustration effects that force them into novel types of ground states not found in superconductors with one or two bands crossing the Fermi surface. In other areas of research, these effects can be found in e.g. spin systems where frustrated spins can give rise to highly degenerate ground states and new symmetries. It will become clear that frustration forces systems to make a "choice" on how to configure themselves, and in the context of superconductors, frustration arising because of the phases of the complex order parameters – *phase frustration* – can lead to the system choosing a configuration which breaks time-reversal symmetry.

2.4.1 Frustration

The term *frustration* will in this thesis be used in the sense that a system is *frustrated* if individual parts of the system prefer to be in different configurations which are incompatible in such a way that it is impossible for all the parts to reach their individual preference [37]. A frustrated system consists of parts with competing preferences, and it has to choose a compromise to "solve" the frustration. One could also establish a local definition and say that an individual part of the system is frustrated when it cannot satisfy all the preferences from interactions with other parts.

As a simple example, we can consider two 2D spins $\mathbf{S}_1, \mathbf{S}_2$ with $|\mathbf{S}_i| = 1$ interacting with strength J so that the Hamiltonian describing the spins is

$$H = J\mathbf{S}_1 \cdot \mathbf{S}_2 = J\cos(\theta_{12}), \tag{2.31}$$

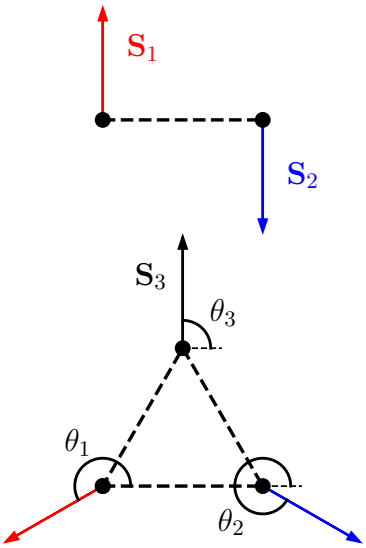

Figure 2.4: Illustration of the ground states of two (top, no frustration) versus three (bottom, frustration on triangular lattice) 2D Heisenberg spins with antiferromagnetic coupling.

where the difference between the angles θ_1, θ_2 the spins make with e.g. the x-axis is $\theta_{12} = \theta_1 - \theta_2$. The spins in a ground state position are illustrated at the top of Fig. 2.4. Depending on the sign of J, the ground state will have either $\mathbf{S}_i$ pointing in opposite directions or the same direction to minimize the energy. In the former case, $J > 0$ and $\theta_{12} = \pi$, we call the interaction *antiferromagnetic*, and in the latter, $\theta_{12} = 0, J < 0$-case, we call it *ferromagnetic*. Let us now assume that $J > 0$ and add another spin, $\mathbf{S}_3$, which interacts with one of the other spins, say $\mathbf{S}_2$, with the same strength, J. The Hamiltonian now has two terms, $J\cos(\theta_{12}) + J\cos(\theta_{23})$, but they can both be minimized at the same time, $\theta_{12} = \theta_{23} = \pi$, leaving the total energy minimized in this case, too. Frustration does not come into play until we let the third spin interact also with the first spin, again with strength J for simplicity. Now,

$$H = J(\cos(\theta_{12}) + \cos(\theta_{23}) + \cos(\theta_{13})), \tag{2.32}$$

and since $\theta_{13} = \theta_{23} + \theta_{12}$, the angle between $\mathbf{S}_1$ and $\mathbf{S}_3$ is forced to be 2π, i.e. 0, if the other spins are to point in opposite directions. Consequently, the last term cannot be minimized while the other two are at their minimum, so the system is frustrated. With the local definition, we could say each interaction term is frustrated, or that we have three frustrated spins. Similarly, this system with three interactions would be frustrated if two interactions were ferromagnetic and one were antiferromagnetic. Then, the ferromagnetic interactions would prefer two of the angle differences to be 0, which would make it impossible to have the third be π. The compromise in the first example, three antiferromagnetic interactions, is to have all the angles between spins be $2\pi/3$. This is illustrated in the bottom part of Fig. 2.4 and can be seen by minimizing the *two*-variable function in Eq. (2.32) [37].

The frustration arising in the three-band systems studied in this thesis will be rather analogous to the above three spins. The gaps $|\Delta_\alpha|$ are analogous to the spins, and the differences in the complex phases of the gaps play the role of the angle differences. A complication not present in the example spin ground state energy is that the factors in front of the cosines will depend on several microscopic parameters of the theory in addition to the gaps. In the example, the cosine prefactors are determined by the interaction strength J and the spin magnitudes $|\mathbf{S}_i|$.

2.4.2 Time reversal

In Newtonian mechanics, one might contemplate "running time backwards", which can be thought of as rewinding the video recording of an experiment, and checking whether the trajectories of particles and the forces involved are still physically permissible. If they are, we say that the system respects *time-reversal symmetry*. Similarly, if a physical law retains the same form under time reversal, we call it *time-reversal invariant*. As is often the case, quantum mechanics complicates matters; in quantum mechanics, we postulate certain behaviors for how the time-reversal operator $\mathcal{T}$ acts on many-particle states in Fock space and its many-particle operators [38]. We will follow Sigrist and Ueda [18], who let $\mathcal{T}$ map the superconducting gap function $\Delta(\mathbf{k})$ to its complex conjugate on the opposite side of momentum space, $\Delta^\dagger(-\mathbf{k})$. Extending this notion to N gaps and collecting the gaps in a vector $\mathbf{\Delta}(\mathbf{k})$ with components $\Delta_\alpha(\mathbf{k})$, we have

$$\mathcal{T}(\mathbf{\Delta}(\mathbf{k})) = \mathbf{\Delta}^*(-\mathbf{k}), \tag{2.33}$$

i.e. each component is complex conjugated and evaluated at the opposite side of $\mathbf{k}$-space. In this thesis, however, the gap functions will be momentum independent, so time reversal will be equivalent to a $\mathbb{Z}_2$ transformation, i.e. a flipping of all gap phases $\theta_\alpha \mapsto -\theta_\alpha$.

What we are interested in is the question of when our superconducting state can *break* time-reversal symmetry. In quantum mechanics, this amounts to asking, "when does $\mathcal{T}$ send $\mathbf{\Delta}$ to a physically distinct state?". As we will see when we derive the gap equations, the overall phase of the gaps does not matter, it is the phase differences that matters, meaning we can rotate all the gaps by the same phase ϕ, $\mathbf{\Delta} \mapsto \mathbf{\Delta}e^{i\phi}$, and still describe the same state. Hence, the state $\mathbf{\Delta}$ *breaks* time-reversal symmetry when there does *not* exist a real number ϕ such that

$$\mathcal{T}(\mathbf{\Delta}) = \mathbf{\Delta}e^{i\phi}. \tag{2.34}$$

When there is only one gap, $\Delta_1 = |\Delta_1|e^{i\theta_1}$, time reversal does not map the system to a different state since rotating the gap by the phase angle $\phi = 2\theta_1$ sends $\mathcal{T}(\Delta_1)$ back to Δ_1. The gap will consequently not break time-reversal symmetry in the one-band case. In the two-band case one might think that TRSB can occur if the gaps form an angle not equal to 0 or π, but we will show in the next chapter that the phase difference $\theta_1 - \theta_2$ must be a multiple of π in mean-field theory. This means that Δ_1 and Δ_2 point in the same or the opposite direction in the complex plane, such that complex conjugation merely rotates both the gaps by the same angle, as can be seen from the illustration in the bottom part of Fig. 2.5. Again, a global phase rotation does not change the physics so the two-band superconductor will not break time-reversal symmetry when mean-field theory applies.

For a three-band superconductor, however, complex conjugation does not necessarily rotate all the gaps by the same angle. This can be seen in the illustration of the gaps in some typical TRSB state, Fig. 2.5. To see it mathematically, let us take e.g. $\Delta_1 = |\Delta_1|$, $\Delta_2 = |\Delta_2|e^{i\theta_2}$, $\Delta_3 = |\Delta_3|e^{i\theta_3}$, where we

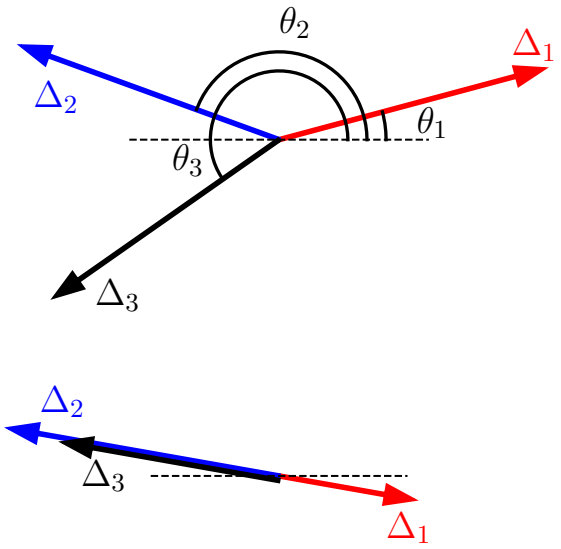

Figure 2.5: Illustrations of the complex superconducting gap functions. The arrow lengths indicate the magnitudes of the gaps whereas the angles indicate the phases. *Top*: A typical TRSB state. Complex conjugation of each gap makes it impossible to $U(1)$ rotate back to the original configuration. *Bottom*: A typical time-reversal symmetric state, the phase differences are 0 and π, so complex conjugation merely rotates all the gaps by the same angle.

have chosen $\theta_1 = 0$ by performing a global phase rotation. If we wish to map $\mathcal{T}(\Delta_2)$ back to Δ_2, we would need $\phi = 2\theta_2$, but the same applies to $\mathcal{T}(\Delta_3)$, now requiring $\phi = 2\theta_3$. Lastly, to bring the real number $\mathcal{T}(\Delta_1)$ back to Δ_1, we would need $\phi = 2n\pi$ for some integer n. This forces θ_2 and θ_3 to be integer multiples of π, such that a $\mathbf{\Delta}$ where any of the phase differences is different from 0 or π will break time-reversal symmetry.

Chapter 3

Gap equations and free energy

We have now seen how the phase differences of the complex gap functions play a crucial role in the question of whether or not a superconductor breaks time-reversal symmetry. Turning our attention to these phases, we now diagonalize the Hamiltonian in order to calculate the free energy of a three-band superconductor and derive the gap equations. At the end of the chapter, we will make some remarks on how one might get TRSB from the microscopic parameters of the theory.

3.1 Diagonalization of the Hamiltonian and its excitation spectrum

The Hamiltonian in Eq. (2.30) is not written in a form where we can read off the excitation spectrum of the system due to the anomalous terms $c_{-\mathbf{k}\downarrow\alpha}c_{\mathbf{k}\uparrow\alpha}$ and $c^\dagger_{\mathbf{k}\uparrow\alpha}c^\dagger_{-\mathbf{k}\downarrow\alpha}$. We can, however remove these terms by performing a rotation – a Bogoliubov transformation [36] – of the creation and destruction operators so as to retain only terms which are in the form of a number operator. There are several ways to do this, both in terms of how one constructs the new fermion operators and how many assumptions one makes about the transformation coefficients. The choice made here is to introduce the operators

$$\begin{aligned}\zeta^\dagger_{\mathbf{k}\alpha} &= v^*_{\mathbf{k}\alpha}c_{-\mathbf{k}\downarrow\alpha} + u^*_{\mathbf{k}\alpha}c^\dagger_{\mathbf{k}\uparrow\alpha}\\ \gamma^\dagger_{\mathbf{k}\alpha} &= u_{\mathbf{k}\alpha}c_{-\mathbf{k}\downarrow\alpha} - v_{\mathbf{k}\alpha}c^\dagger_{\mathbf{k}\uparrow\alpha},\end{aligned} \tag{3.1}$$

where $u_{\mathbf{k}\alpha}, v_{\mathbf{k}\alpha}$ are complex numbers. One could have chosen four complex numbers, one for each operator term in Eq. (3.1), but for the purposes of this thesis and the model studied here, it suffices to use $u_{\mathbf{k}\alpha}, v_{\mathbf{k}\alpha}$ in order to get complex gaps Δ_α with nontrivial phases and phase differences. Had we chosen $u_{\mathbf{k}\alpha}, v_{\mathbf{k}\alpha}$ real, the phase differences would have been trivial and the physics of interest related to phase frustration would not have emerged naturally from the microscopic Hamiltonian we are presently investigating at the mean-field level. In other words, real $u_{\mathbf{k}\alpha}, v_{\mathbf{k}\alpha}$ would force us to put in nontrivial phases of Δ_α as a solution by hand. This fact will be shown explicitly below.

We demand that the new operators be fermion operators, namely that

$$\left\{\zeta^\dagger_{\mathbf{k}\alpha}, \zeta_{\mathbf{k}'\beta}\right\} = \delta_{\mathbf{k}\mathbf{k}'}\delta_{\alpha\beta} \tag{3.2}$$

$$\left\{\eta^\dagger_{\mathbf{k}\alpha}, \eta_{\mathbf{k}'\beta}\right\} = \delta_{\mathbf{k}\mathbf{k}'}\delta_{\alpha\beta} \tag{3.3}$$

and $\{\zeta_{\mathbf{k}\alpha}, \zeta_{\mathbf{k}'\beta}\} = 0 = \{\eta_{\mathbf{k}\alpha}, \eta_{\mathbf{k}'\beta}\}$. The consequence of both Eq. (3.2) and (3.3) is that the transformation coefficients must obey

$$|u_{\mathbf{k}\alpha}|^2 + |v_{\mathbf{k}\alpha}|^2 = 1, \tag{3.4}$$

which later will allow us to use the parametrization

$$\begin{aligned} u_{\mathbf{k}\alpha} &= \cos(\Phi_{\mathbf{k}\alpha})\mathrm{e}^{i\vartheta_{\mathbf{k}\alpha}} \\ v_{\mathbf{k}\alpha} &= \sin(\Phi_{\mathbf{k}\alpha})\mathrm{e}^{i\varphi_{\mathbf{k}\alpha}}, \end{aligned} \tag{3.5}$$

where the angle parameters $\Phi_{\mathbf{k}\alpha}, \vartheta_{\mathbf{k}\alpha}, \varphi_{\mathbf{k}\alpha} \in \mathbb{R}$ will be chosen in such a way that they leave H diagonal. Inverting Eq. (3.1) by making use of Eq. (3.4), we obtain

$$\begin{aligned} c_{\mathbf{k}\uparrow\alpha} &= u^*_{\mathbf{k}\alpha}\zeta_{\mathbf{k}\alpha} - v_{\mathbf{k}\alpha}\gamma_{\mathbf{k}\alpha} \\ c^\dagger_{-\mathbf{k}\downarrow\alpha} &= v^*_{\mathbf{k}\alpha}\zeta_{\mathbf{k}\alpha} + u_{\mathbf{k}\alpha}\gamma_{\mathbf{k}\alpha}, \end{aligned} \tag{3.6}$$

which can be inserted into the Hamiltonian (2.29), yielding

$$\begin{aligned} H = \tilde{E}_0 + \sum_{\mathbf{k},\alpha}\Big\{ & E_{\mathbf{k}\alpha}\left[\gamma^\dagger_{\mathbf{k}\alpha}\gamma_{\mathbf{k}\alpha} - \zeta^\dagger_{\mathbf{k}\alpha}\zeta_{\mathbf{k}\alpha}\right] + \tilde{\varepsilon}_{\mathbf{k}\alpha} \\ & + \left[-2\tilde{\varepsilon}_{\mathbf{k}\alpha}u_{\mathbf{k}\alpha}v_{\mathbf{k}\alpha} - \Delta_\alpha(\mathbf{k})u^2_{\mathbf{k}\alpha} + \Delta^\dagger_\alpha(\mathbf{k})v^2_{\mathbf{k}\alpha}\right]\zeta^\dagger_{\mathbf{k}\alpha}\gamma_{\mathbf{k}\alpha} + \text{h.c.}\Big\} \end{aligned} \tag{3.7}$$

by collecting terms and anticommuting the necessary pairs of operators. The excitation energy $E_{\mathbf{k}\alpha}$, which appears with a negative sign for the first species of quasiparticles, $\zeta^\dagger_{\mathbf{k}\alpha}$ and a positive sign for the other, is

$$E_{\mathbf{k}\alpha} = \tilde{\varepsilon}_{\mathbf{k}\alpha}\cos(2\Phi_{\mathbf{k}\alpha}) + \mathrm{Re}\left(\tilde{\Delta}_\alpha(\mathbf{k})\right)\sin(2\Phi_{\mathbf{k}\alpha}), \tag{3.8}$$

where we have defined the quantity

$$\tilde{\Delta}_\alpha(\mathbf{k}) = \Delta_\alpha(\mathbf{k})\mathrm{e}^{i(\vartheta_{\mathbf{k}\alpha}-\varphi_{\mathbf{k}\alpha})}. \tag{3.9}$$

We now diagonalize H by demanding that the coefficients of the anomalous operator pairs in the second line of Eq. (3.8) be zero. These demands are equivalent as the resulting equations are complex conjugates of each other. They lead to the conclusion that the quantity defined above

$$\tilde{\Delta}_\alpha(\mathbf{k}) \in \mathbb{R}, \tag{3.10}$$

in addition to the equation

$$\frac{\tilde{\Delta}_\alpha(\mathbf{k})}{\tilde{\varepsilon}_{\mathbf{k}\alpha}} = \tan(2\Phi_{\mathbf{k}\alpha}) \tag{3.11}$$

when $\Delta_\alpha(\mathbf{k}) \neq 0$ and

$$\sin(2\Phi_{\mathbf{k}\alpha}) = 0 \tag{3.12}$$

when $\Delta_\alpha(\mathbf{k}) = 0$. Here, a remark about Eq. (3.10) is in order. We see from Eq. (3.9) that if we had chosen the Bogoliubov transformation coefficients to be real, $\vartheta_{\mathbf{k}\alpha} = n\pi, \varphi_{\mathbf{k}\alpha} = m\pi$ for integers n, m, then $\Delta_\alpha(\mathbf{k})$ would have been forced to to be real. With our choice, however, the complex phases of the gap functions are preserved, and, as we will see, the phases of the transformation coefficients will essentially disappear from the problem.

Let us use the diagonalization criterion, Eq. (3.11), to express the quasiparticle excitation energies in terms of $\tilde{\varepsilon}_{\mathbf{k}\alpha}$ and $|\Delta_\alpha(\mathbf{k})|$. The right-hand side of Eq. (3.11) is π-periodic in $2\Phi_{\mathbf{k}\alpha}$, so a choice of $2\Phi_{\mathbf{k}\alpha}$-interval must be made, and depending on the choice, the excitation energies will look slightly different. For $2\Phi_{\mathbf{k}\alpha} \in [-\pi/2, \pi/2)$, they will switch sign when $\tilde{\varepsilon}_{\mathbf{k}\alpha}$ does because in this case,

$$\begin{aligned} E_{\mathbf{k}\alpha} &= \mathrm{sgn}\left(\tilde{\varepsilon}_{\mathbf{k}\alpha}\right)\left(\tilde{\varepsilon}^2_{\mathbf{k}\alpha} + |\Delta_\alpha(\mathbf{k})|^2\right)^{1/2} \\ \cos(2\Phi_{\mathbf{k}\alpha}) &= |\tilde{\varepsilon}_{\mathbf{k}\alpha}|\left(\tilde{\varepsilon}^2_{\mathbf{k}\alpha} + |\Delta_\alpha(\mathbf{k})|^2\right)^{-1/2}. \end{aligned} \tag{3.13}$$

For $2\Phi_{\mathbf{k}\alpha} \in [0, \pi)$, on the other hand,

$$\begin{aligned} E_{\mathbf{k}\alpha} &= \operatorname{sgn}\left(\tilde{\Delta}_\alpha(\mathbf{k})\right)\left(\tilde{\varepsilon}^2_{\mathbf{k}\alpha} + |\Delta_\alpha(\mathbf{k})|^2\right)^{1/2} \\ \cos(2\Phi_{\mathbf{k}\alpha}) &= \operatorname{sgn}\left(\tilde{\Delta}_\alpha(\mathbf{k})\right)\tilde{\varepsilon}_{\mathbf{k}\alpha}\left(\tilde{\varepsilon}^2_{\mathbf{k}\alpha} + |\Delta_\alpha(\mathbf{k})|^2\right)^{-1/2}. \end{aligned} \tag{3.14}$$

In both cases, $\sin(2\Phi_{\mathbf{k}\alpha}) = \tilde{\Delta}_\alpha(\mathbf{k})/E_{\mathbf{k}\alpha}$ for the corresponding $E_{\mathbf{k}\alpha}$-expression and $E_{\mathbf{k}\alpha} = \tilde{\varepsilon}_{\mathbf{k}\alpha}$ when $\mathbf{k} \notin F_\alpha$. Additionally, we can now identify that the gap functions indeed represent a *gap*. The quasiparticle energies have a gap, given by $|\Delta_\alpha|$, near the Fermi surface, meaning the system is protected from the resistivity-causing scattering from energy states right below the Fermi surface to above it and that the electrons can move frictionlessly [5]. In the rest of the thesis, we will use the first $2\Phi_{\mathbf{k}\alpha}$-interval and the expression for the excitation energies given in Eq. (3.13) along with our now diagonalized Hamiltonian in the form of a constant mean-field term E_0 added to a gas of free fermions,

$$H = E_0 + \sum_{\mathbf{k},\alpha} E_{\mathbf{k}\alpha}\left(\gamma^\dagger_{\mathbf{k}\alpha}\gamma_{\mathbf{k}\alpha} - \zeta^\dagger_{\mathbf{k}\alpha}\zeta_{\mathbf{k}\alpha}\right), \tag{3.15}$$

$$E_0 = \sum_{\mathbf{k},\alpha} \tilde{\varepsilon}_{\mathbf{k}\alpha} + \sum_{\mathbf{k},\mathbf{k}',\alpha,\beta} V_{\alpha\beta}(\mathbf{k},\mathbf{k}')b^\dagger_{\mathbf{k}\alpha}b_{\mathbf{k}'\beta} \tag{3.16}$$

with reference to Eq. (2.22) for the expression for $\tilde{E}_0$. As a final note, we rewrite E_0 to

$$E_0 = \sum_{\mathbf{k},\alpha} \tilde{\varepsilon}_{\mathbf{k}\alpha} + \sum_{\alpha,\beta} b^\dagger_\alpha V_{\alpha\beta} b_\beta \tag{3.17}$$

$$= \sum_{\mathbf{k},\alpha} \tilde{\varepsilon}_{\mathbf{k}\alpha} + \sum_{\alpha,\beta} \Delta^\dagger_\alpha V^{-1}_{\alpha\beta}\Delta_\beta \tag{3.18}$$

using the definitions (2.26) and (2.27), the fact that $\mathbf{b} = \mathbf{V}^{-1}\mathbf{\Delta}$, and the definition $V^{-1}_{\alpha\beta} = (\mathbf{V}^{-1})_{\alpha\beta}$.

3.2 Free energy

The Helmholtz free energy F of our system can be calculated in the grand canonical ensemble since all ensembles are equivalent in the thermodynamic limit of particle number N and system volume V going to infinity while keeping N/V constant [34]. For a grand canonical ensemble at temperature $T = 1/k_\mathrm{B}\beta$ with chemical potential $\tilde{\mu}$, the free energy is

$$F = -\frac{1}{\beta}\ln(Z_\mathrm{G}) + \frac{\tilde{\mu}}{\beta}\frac{\partial(\ln Z_\mathrm{G})}{\partial\tilde{\mu}}, \tag{3.19}$$

where the the grand canonical partition function is

$$Z_\mathrm{G} = \operatorname{Tr}\left(\mathrm{e}^{-\beta(H-\tilde{\mu}N)}\right), \tag{3.20}$$

and we do not distinguish between operators and numbers. Here, H is the Hamiltonian operator of the system and N is the number operator.

In the present case, the Hamiltonian is given in Eq. (3.15) and $\tilde{\mu} = 0$ for the quasiparticles. Let us begin by labeling the fermion energy eigenstates $|n_1 \dots n_N\rangle = |n_1\rangle \otimes \dots \otimes |n_N\rangle$ for notational simplicity. The number operator is not necessary here since $\tilde{\mu} = 0$, so we use N as the number of possible states. Therefore, if state number i corresponds to e.g. a ζ quasiparticle with momentum $\mathbf{k}$ being in orbital α, then $H|n_i\rangle = E_{n_i}|n_i\rangle = -E_{\mathbf{k}\alpha}|n_i\rangle$, where we have $E_{n_i} = -E_{\mathbf{k}\alpha}$ from Eq. (3.15). Here, the number n_i

can only be 1 or 0 because the quasiparticles are fermions. Thus, the partition function is

$$\begin{aligned} Z_{\mathrm{G}} &= \sum_{n_1,\ldots,n_N} \langle n_1 \ldots n_N | \, \mathrm{e}^{-\beta H} \, | n_1, \ldots, n_N \rangle \\ &= \sum_{n_1 \ldots n_N} \langle n_1 \ldots n_N | \exp\left[-\beta \left(E_0 + \sum_i E_{n_i} n_i \right) \right] | n_1 \ldots n_N \rangle \\ &= \mathrm{e}^{-\beta E_0} \sum_{n_1=0}^{1} \langle n_1 | \, \mathrm{e}^{-\beta E_{n_1} n_1} \, | n_1 \rangle \ldots \sum_{n_N=0}^{1} \langle n_N | \, \mathrm{e}^{-\beta E_{n_N} n_N} \, | n_N \rangle \\ &= \mathrm{e}^{-\beta E_0} \prod_{\mathbf{k},\alpha} \left(1 + \mathrm{e}^{-\beta E_{\mathbf{k}\alpha}} \right) \left(1 + \mathrm{e}^{\beta E_{\mathbf{k}\alpha}} \right), \end{aligned} \tag{3.21}$$

from which we calculate the free energy

$$F = E_0 - \frac{1}{\beta} \sum_{\mathbf{k},\alpha} \left[\ln\left(1 + \mathrm{e}^{-\beta E_{\mathbf{k}\alpha}} \right) + \ln\left(1 + \mathrm{e}^{\beta E_{\mathbf{k}\alpha}} \right) \right] \tag{3.22}$$

which has to be minimal at thermal equilibrium. In the case of an N-band superconductor, we therefore get N equations $\partial F / \partial \Delta_\nu = 0$ which we will now explore.

3.2.1 Gap equations guarantee an extremized free energy

There are multiple ways to arrive at the gap equations. One is to use the the definition (2.28) directly and determine the gaps self-consistently by inserting the new quasiparticle operators into the thermal averages $b_{\mathbf{k}\alpha}, b^\dagger_{\mathbf{k}\alpha}$. Perhaps more illuminatingly, one can set the differential of the free energy with respect to some set of variational parameters of the theory to zero. To avoid confusion or errors, one should keep F expressed in terms of only one set of parameters at the time. We will use the momentum-independent gaps Δ_α, but we could also have used the parameters b_α which would have yielded the same result, except with a little longer derivation. The N equations $\partial F / \partial \Delta_\nu = 0$ applied to the free energy in Eq. (3.22) are

$$0 = \frac{\partial E_0}{\partial \Delta_\nu} - \sum_{\mathbf{k} \in F_\nu} \frac{\partial E_{\mathbf{k}\nu}}{\partial \Delta_\nu} \tanh\left(\frac{\beta E_{\mathbf{k}\nu}}{2} \right), \tag{3.23}$$

where the momentum sum is restricted to only contain terms in the momentum shell around Fermi surface ν as $E_{\mathbf{k}\alpha}$ is simply equal to $\tilde{\varepsilon}_{\mathbf{k}\alpha}$ elsewhere. Using Eq. (3.18) for E_0 and (3.13) for the excitation energies, we obtain

$$\Delta^\dagger_\nu \sum_{\mathbf{k} \in F_\nu} \frac{1}{2E_{\mathbf{k}\nu}} \tanh\left(\frac{\beta E_{\mathbf{k}\nu}}{2} \right) = \sum_\beta V^{-1}_{\nu\beta} \Delta^\dagger_\beta \equiv b^\dagger_\nu, \tag{3.24}$$

with reference to the equation $\mathbf{b} = \mathbf{V}^{-1}\mathbf{\Delta}$. The complex conjugate of Eq. (3.24) can now be inserted into the definition of the gaps, $\mathbf{\Delta} = \mathbf{V}\mathbf{b}$, from which we obtain

$$\Delta_\alpha = \sum_\beta \Delta_\beta V_{\alpha\beta} \sum_{\mathbf{k} \in F_\beta} \frac{1}{2E_{\mathbf{k}\beta}} \tanh\left(\frac{\beta E_{\mathbf{k}\beta}}{2} \right). \tag{3.25}$$

The signs in the denominator and argument of the tanh function cancel, and because the momentum sum runs over momenta in F_β, all the $\mathbf{k}$ dependence is in the single-particle excitation energies $\tilde{\varepsilon}_{\mathbf{k}\beta}$. Thus, we can convert the sum to an energy integral, assume that the single-particle density of states $N_\beta(\tilde{\varepsilon})$ can be approximated to its value $N_\beta(0)$ at the Fermi surface, and finally arrive at the gap equations for our N-band superconductor:

$$\Delta_\alpha = \sum_\beta V_{\alpha\beta} \Delta_\beta N_\beta(0) S_\beta. \tag{3.26}$$

Here, the energy integral is

$$S_\alpha = \int_0^{\omega_\alpha} \mathrm{d}\tilde{\varepsilon} \left(\tilde{\varepsilon}^2 + |\Delta_\alpha|^2\right)^{-1/2} \tanh\left[\frac{\beta}{2}\left(\tilde{\varepsilon}^2 + |\Delta_\alpha|^2\right)^{1/2}\right], \tag{3.27}$$

where the symbol β means inverse temperature only in the hyperbolic tangent function where it is divided by two.

At this point, the claim about two-band superconductors made in section 2.4.2 can be substantiated. If we first rewrite the gap equations

$$|\Delta_\alpha| = \sum_\beta V_{\alpha\beta}|\Delta_\beta| \mathrm{e}^{i\theta_{\beta\alpha}} N_\beta(0) S_\beta, \tag{3.28}$$

it becomes clear that only the phase *differences*, $\theta_{\alpha\beta} = \theta_\alpha - \theta_\beta$, have any significance and that an overall $U(1)$ rotation of the gaps does not affect the physics. In the case of $N = 2$ bands, taking the imaginary part of e.g. the first equation,

$$|\Delta_1| = V_{11} S_1 N_1(0) |\Delta_1| + V_{12} S_2 N_2(0) |\Delta_2| \mathrm{e}^{-i\theta_{12}}, \tag{3.29}$$

leads to

$$\sin\theta_{12} = 0, \tag{3.30}$$

forcing the phase difference to be an integer multiple of π. In effect, one can then set $\Delta_\alpha \in \mathbb{R}$, as claimed; the phases can be encapsulated in the sign of the gaps.

3.3 Frustration and TRSB in multiband superconductors

We will soon solve the gap equations numerically in search of TRSB, but let us first construct parts of a road map to help navigate the vast parameter space of $\{V_{\alpha\beta}, \tilde{\varepsilon}_{\mathbf{k}\alpha}, N_\alpha(0), \omega_\alpha\}$. The first step in doing this is to look for some minimum requirements we can place on the microscopic parameters. After that, some more general constraints are stated before we begin making simplifications allowing us to find specific examples of combinations of parameters that break time-reversal symmetry.

3.3.1 Minimum requirements for TRSB

The statement made at the end of section 3.2.1 can be made in a different way by analyzing the gap equations for $N = 3$. If the e.g. the third band is empty, $N_3(0) = 0$,[1] the imaginary part of the first gap equation states that

$$V_{12} N_2(0) S_2 |\Delta_2| \sin(\theta_{12}) + V_{13} N_3(0) S_3 |\Delta_3| \sin(\theta_{13}) = 0, \tag{3.31}$$

i.e. $\sin(\theta_{12}) = 0$. This propagates to the third equation, whose imaginary part amounts to $\sin(\theta_{13}) = 0$, again showing that with only two energy bands, real-valued gap functions suffice.

A slightly more subtle point regarding the three-band case is that setting any single interband coupling $V_{\alpha\beta} = 0$ for $\alpha \neq \beta$ will also lead to a stillborn attempt at finding TRSB.[2] We can without loss of generality take $V_{23} = 0$ to justify this claim. The imaginary parts of the second and third gap equation,

$$\begin{aligned} V_{12} N_1(0) S_1 |\Delta_1| \sin(\theta_{12}) + V_{23} N_3(0) S_3 |\Delta_3| \sin(\theta_{12} - \theta_{13}) &= 0, \\ V_{13} N_1(0) S_1 |\Delta_1| \sin(\theta_{13}) - V_{23} N_2(0) S_2 |\Delta_2| \sin(\theta_{12} - \theta_{13}) &= 0, \end{aligned} \tag{3.32}$$

clearly force $\sin(\theta_{\alpha\beta}) = 0$ for all $\alpha \neq \beta$. Accordingly, a prerequisite for TRSB is that the system can have pair tunneling between all pairs of bands, not just that each band is coupled to another band. Equivalently, if the momentum-space "circuit" $1 \leftrightarrow 2 \leftrightarrow 3 \leftrightarrow 1$ is not closed, there will be no TRSB.

[1] This happens if $\mu(t)$ is below the bottom of band three in Fig. 2.3a.

[2] Using our assumption that $V_{\alpha\beta} = V_{\beta\alpha}$.

Some slightly less explicit requirements can also be gleaned from the free energy (3.22). Upon examination, one quickly realizes that it has only one phase-dependent term, to wit, $\tilde{E}_0$ which was defined after Eq. (2.22). As noted in Eq. (3.18), this ground state energy can be written in terms of the gaps. The form

$$\tilde{E}_0 = \sum_\alpha V_{\alpha\alpha}^{-1}|\Delta_\alpha|^2 + 2\sum_{\alpha>\beta} V_{\alpha\beta}^{-1}|\Delta_\alpha\Delta_\beta|\cos(\theta_{\alpha\beta}), \tag{3.33}$$

with $\theta_{\alpha\beta} = \theta_\alpha - \theta_\beta$, is particularly helpful. This is the analogy with the Heisenberg spins mentioned in section 2.4.1 because when we consider the $N = 3$-band case,

$$\begin{aligned}\tilde{E}_0 = \sum_{\alpha=1}^{3} V_{\alpha\alpha}^{-1}|\Delta_\alpha|^2 &+ 2V_{12}^{-1}|\Delta_1\Delta_2|\cos(\theta_{12}) \\ &+ 2V_{13}^{-1}|\Delta_1\Delta_3|\cos(\theta_{13}) \\ &+ 2V_{23}^{-1}|\Delta_2\Delta_3|\cos\underbrace{(\theta_{13}-\theta_{12})}_{\theta_{23}},\end{aligned} \tag{3.34}$$

whereas in the two-band case

$$\tilde{E}_0 = \sum_{\alpha=1}^{2} V_{\alpha\alpha}^{-1}|\Delta_\alpha|^2 + 2V_{12}^{-1}|\Delta_1\Delta_2|\cos(\theta_{12}). \tag{3.35}$$

Both of these equations illustrate the fact that the ground-state energy is $\mathbb{Z}_2$ symmetric in the phases or phase differences; changing $\theta_{\alpha\beta} \mapsto -\theta_{\alpha\beta}$ yields the same energy, but possibly a physically distinct state if the phases are nontrivial.

Returning to the point about the spin analogy, we see that in the two-band case, $\tilde{E}_0$, and thus F, is minimized with respect to the phase difference θ_{12} when it is 0 or π, depending on the sign of the inverse interaction matrix element V_{12}^{-1}. No frustration or TRSB there, in other words. When we go to the three-band case, however, there are, as pointed out in Ref. [29], two combinations of the *signs* of $V_{\alpha\beta}^{-1}$ that make the ground state frustrated. One is if all are positive (all antiferromagnetic interactions in the analogy), and the other is if two are negative and the other positive (one antiferromagnetic and two ferromagnetic). The latter case can obviously be realized in multiple ways, but to keep things simple, one can treat them as the same and relabel the energy bands at a later time. To connect the present discussion to the notation used for the coefficients of the cosines in the GL free energies in previous studies [29, 31], we define

$$g_{\alpha\beta} = 2V_{\alpha\beta}^{-1}|\Delta_\alpha||\Delta_\beta|. \tag{3.36}$$

Now, the other sign combinations for $g_{\alpha\beta}$, $---$ and $-++$, cannot lead to TRSB. With the former combination, all phase differences lock to $\theta_{\alpha\beta} = 0$. In the latter, the two cosines with the plus signs get a phase difference of π, meaning the third, which is a linear combination of the other differences, will get a phase difference of 0 $(\mathrm{mod}\, 2\pi)$. No set of gaps yielding these sign combinations will be affected by time reversal, as we have seen.

To make the connection between phase frustration and the microscopic theory parameters abundantly clear, we reiterate the fact that phase frustration is controlled by the signs of $g_{\alpha\beta}$ for $\alpha \neq \beta$. As a consequence, phase frustration is determined entirely by 1) the determinant of $\mathbf{V}$, printed here in the three-band case for reference,

$$\det\mathbf{V} = V_{11}V_{22}V_{33} - V_{12}^2V_{33} - V_{13}^2V_{22} - V_{23}^2V_{11} + 2V_{12}V_{13}V_{23}, \tag{3.37}$$

and 2) linear combinations of squares of $V_{\alpha\beta}$ since

$$\begin{aligned}V_{\alpha\alpha}^{-1} &= \frac{1}{\det\mathbf{V}}(V_{\beta\beta}V_{\gamma\gamma} - V_{\beta\gamma}^2), \\ V_{\alpha\beta}^{-1} &= \frac{1}{\det\mathbf{V}}(V_{\alpha\gamma}V_{\beta\gamma} - V_{\alpha\beta}V_{\gamma\gamma}),\end{aligned} \tag{3.38}$$

with all α, β, γ unequal. The constraints on the couplings come from

$$V_{\alpha\alpha}^{-1} \geq 0 \tag{3.39}$$

and whichever sign combination one chooses for $V_{\alpha\beta}^{-1}$, or equivalently, $g_{\alpha\beta}$. Eq. (3.39) ensures that the free energy cannot take on arbitrarily low negative values for large $|\Delta_\alpha|$. No other terms in Eq. (3.22) scale as $|\Delta_\alpha|^2$ for large $|\Delta_\alpha|$, so mean-field theory does not make sense for $V_{\alpha\alpha}^{-1} < 0$.

3.3.2 *g*'s and some configurations which yield TRSB

This section is a slight expansion of Fig. 4 in [31]. Therein, the authors studied two equal cosine prefactors, $g_{12} = g_{13} \equiv g$ and one variable, g_{23}. This problem can be treated analytically. The phase-dependent part of the ground-state energy is

$$g\left(\cos(\theta_{12}) + \cos(\theta_{13})\right) + g_{23}\cos(\theta_{13} - \theta_{12}). \tag{3.40}$$

Setting the partial derivatives of the function in Eq. (3.40) to zero and applying the second derivative test shows three sets of possible minima. The first consists of the minimum $(\theta_{12}, \theta_{13}) = (\pi, \pi)$, the second of $(0, 0)$ and the third is the set of minima $(\phi_0, 2\pi - \phi_0)$ where

$$\phi_0 = \cos^{-1}\left(\frac{-g}{2g_{23}}\right). \tag{3.41}$$

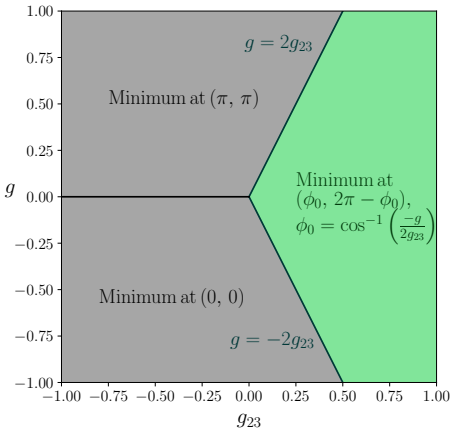

Figure 3.1: Illustration of where the minimum $(\phi_0, 2\pi - \phi_0)$ of the free energy's phase-difference dependent part is for different values of the numbers g and g_{23} which emerge from the microscopic theory. The green region is where time-reversal symmetry is broken.

Clearly, only the last set yields a TRSB state as long as $g \neq 0$. The areas of (g, g_{23})-space where these minima are indeed minima and not maxima or saddle points are shown in Fig. 3.1. As the figure indicates, there are no overlaps except where $|g| = 2g_{23}$, which is uninteresting. We also recognize the above statements about the signs of $g_{\alpha\beta}$. Only $+++$ and $+--$ appear in the green region where TRSB is present. Plotting ϕ_0 as a function of g/g_{23} will in fact yield the same graph as that shown in Fig. 4 in [31] and the curve θ_{23} in Fig. 4.5 in this thesis. This chart can be used as a starting point for investigating TRSB microscopically by finding parameters which make two $g_{\alpha\beta}$'s equal first and specializing to three unequal $g_{\alpha\beta}$'s later.

Chapter 4

Numerical results

In this chapter, we briefly explain how the numerical calculations were set up and performed before moving on to the results. The equation solver is first tested for $N = 2$ bands and compared to the seminal two-band paper of Suhl et al. [9], before moving on to demonstrations that the solver can obtain seemingly different critical temperatures for the two gaps. The model's limitations are also tested, as gaps of the same order of magnitude as the energy cutoff ω are found for certain intraband potentials and densities of states. Here one finds that the gaps do not go to zero near the predicted critical temperature from Suhl et al.'s formula.

4.1 Numerical methods

If we introduce the dimensionless variables

$$\begin{aligned} \Delta'_\alpha &= \Delta_\alpha/\omega_\alpha, \\ V'_{\alpha\beta} &= V_{\alpha\beta}\sqrt{N_\alpha(0)N_\beta(0)}, \\ N'_{\alpha\beta} &= N_\alpha(0)/N_\beta(0), \\ \omega_{\alpha\beta} &= \omega_\alpha/\omega_\beta \end{aligned} \tag{4.1}$$

the gap equations can be written in the dimensionless form

$$\Delta'_\alpha = \sum_\beta \Delta'_\beta V'_{\alpha\beta} N'^{1/2}_{\beta\alpha} \omega'_{\beta\alpha} S'_\beta, \tag{4.2}$$

with

$$S'_\alpha = \int_0^1 \mathrm{d}x \left(x^2 + |\Delta'_\alpha|^2\right)^{-1/2} \tanh\left[\frac{\beta\omega_\alpha}{2}\left(x^2 + |\Delta'_\alpha|^2\right)^{1/2}\right], \tag{4.3}$$

where one can rewrite $\beta\omega_\alpha$ using a dimensionless inverse temperature $\beta' = \beta\omega_{\alpha_{\max}}$ for $\omega_{\alpha_{\max}} \geq \omega_\alpha$ for all $\alpha = 1, ..., N$. To solve the equations for the gaps Δ'_α, then, one must specify the ratios $N'_{\alpha\beta}$ and $\omega'_{\alpha\beta}$, the strength of the interactions compared to the densities of states $V'_{\alpha\beta}$, and the temperature compared to the largest energy shell width β'. To avoid repetition throughout the chapter, we note here that we set $\omega_\alpha = \omega$, i.e. $\omega_{\alpha\beta} = 1$, in all the calculations below. This is no essential simplification, the solver can accommodate different energy cutoffs.

Whenever $T \neq 0$, the numerical energy integrals, S'_α, were calculated with an absolute error tolerance of 1.49×10^{-8}, several orders of magnitude smaller than the integral. The Python numerical equation solver `scipy.optimize.fsolve` was run with a relative error tolerance of 1.49012×10^{-10}. Differences of that order of magnitude are insignificant for the results presented herein. As trial solutions for the equation solver, known analytical expressions for decoupled superconductors were used where possible. In the

calculations where potentials, temperature, or densities of states were changed gradually, the numerical solution from the last iteration was used as the trial solution, again using an analytical expression for the gaps at no coupling and a guess for the phases as the trial solution for the first iteration.

It should be noted that care must be taken not to enter trial phase differences that lie too close to maxima or saddle points of the free energy – the gap equations only find points of zero derivative in the free energy. To avoid this problem, we performed a second derivative test after each iteration by calculating $g_{\alpha\beta}$ from Eq. (3.36) and checking whether the point $(\theta_{12}, \theta_{13})$ corresponded to a minimum of the phase-difference dependent part of F. If it did not, the iteration was run again with new phase differences[1] as trial solutions.

With the exception of the comparison values in Fig. 4.1a, all figures were produced by solving the *five* $N = 3$-band gap equations. These are found by taking the real and imaginary part of the equation for each gap α multiplied by $\exp(-i\theta_\alpha)$,

$$|\Delta'_\alpha| = \sum_\beta \left|\Delta'_\beta\right| e^{i\theta_{\beta\alpha}} V'_{\alpha\beta} N'^{1/2}_{\beta\alpha} \omega'_{\beta\alpha} S'_\beta, \tag{4.4}$$

and discarding one of the imaginary-part equations as the right-hand side of Eq. (4.4) ends up only depending on two phase *differences*. We chose to work with the differences θ_{12} and θ_{13}, using the expression $\theta_{23} = \theta_{13} - \theta_{12}$ where necessary.

4.2 Numerical checks - from two bands to three

An initial test of the equation solver was performed by setting the dimensionless potential $V'_{12} = 1/3$ and the intraband potentials $V'_{11} = V'_{22} = 0$ just like Suhl et al. did in 1959 [9]. The results are shown in Fig. 4.1 for the same ratios N'_{21} used by Suhl. We used their zero-temperature data, shown as crosses in Fig. 4.1a, as the trial solution for each density of states ratio. The word "implicit" in Fig. 4.1a refers to the way in which the equations were solved. Implicit means that the full, complex three-band gap equations were used with $V_{13} = V_{23} = V_{33} = 0$, whereas explicit means the real-valued $N = 2$-band equations were used. The "explicit" data is not shown, but it coincides with the data shown here within the numerical accuracy of the solver.

The gaps in the left plot exhibit the same behavior as in the old Suhl article, except near $T = 0$, where they in our case come out much flatter. They were all slightly lower than Suhl's values, but the deviation was always less than about $0.1 k_B T_c$. This example is rather artificial, as Fig. 4.1b shows, and only served as a test of the equation solver. The figure shows the variation in the dimensionless free energy around the solutions $\left|\Delta_\alpha^{\text{G.E.}}\right|$ of the gap equations, revealing that the energy could have been lowered by either a larger or smaller gap; the gap equations found a local maximum.

The next numerical check involved Suhl et al.'s qualitative diagram showing how the critical temperatures of two decoupled superconductors merge when the coupling is turned on. This has been replicated in Fig. 4.2 with a weakly attractive interband potential $V'_{12} = 10^{-3}$ and for a few different intraband potentials using $N_1(0) = N_2(0) = \text{const}$. The dots along the T-axis indicate where the critical temperature of the smaller gap would be if the coupling had been turned off. For values of $V'_{\alpha\alpha}$ larger than about 0.75, the critical temperatures did not match the point where the gaps went to zero and Δ_1 took on values larger than ω, indicating that the model limit is somewhere between the shown intraband coupling values and the 0.75 value. We will use slightly lower intraband potentials in the following to ensure small enough gaps.

The next step is to turn on the third band and make sure the phase differences come out correctly. We first use $V'_{\alpha\alpha} = 0.2$ and interband interactions several orders of magnitude lower: $V'_{\alpha\beta} = \pm 10^{-5}$. For one interband interaction, which is just a two-band superconductor and a third decoupled superconductor, the phase difference between the coupled ones becomes 0 and π in the correct manner as the sign of the

[1] These new phase differences can be obtained from an analytical expression or e.g. a global optimization algorithm such as `scipy.optimize.dual_annealing`.

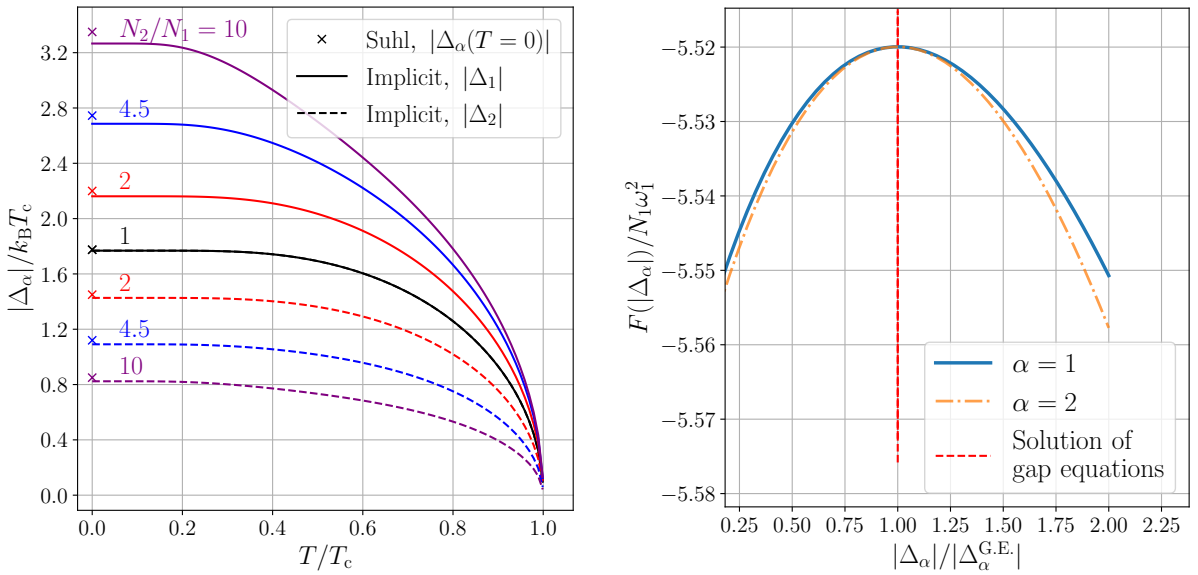

(a) Gap amplitudes obtained by using Suhl et al.'s data as trial solutions in the equation solver and setting the phase difference to 0. Like Suhl et al., we used $V'_{12} = V_{12}\sqrt{N_1(0)N_2(0)} = 1/3$ and $V_{\alpha\alpha} = 0$. The temperature merely approached Suhl et al.'s predicted T_c, so the amplitudes do not reach 0.

(b) Zero-temperature free energy as a function of gap amplitudes near the solution $|\Delta_\alpha^{\mathrm{G.E.}}|$ of the gap equations for the lines $N_2/N_1 = 4.5$ from the left figure. The free energy is maximized as a function of the gap amplitudes, serving as an example that the gap equations extremize the free energy.

Figure 4.1: Solutions of the two-band gap equations for various temperatures and ratios N_2/N_1 between the densities of states at the Fermi surfaces. As in Suhl et al.'s old theory, the phase difference between the bands is 0 here, and the gap equations have lead us to a maximum in the free energy.

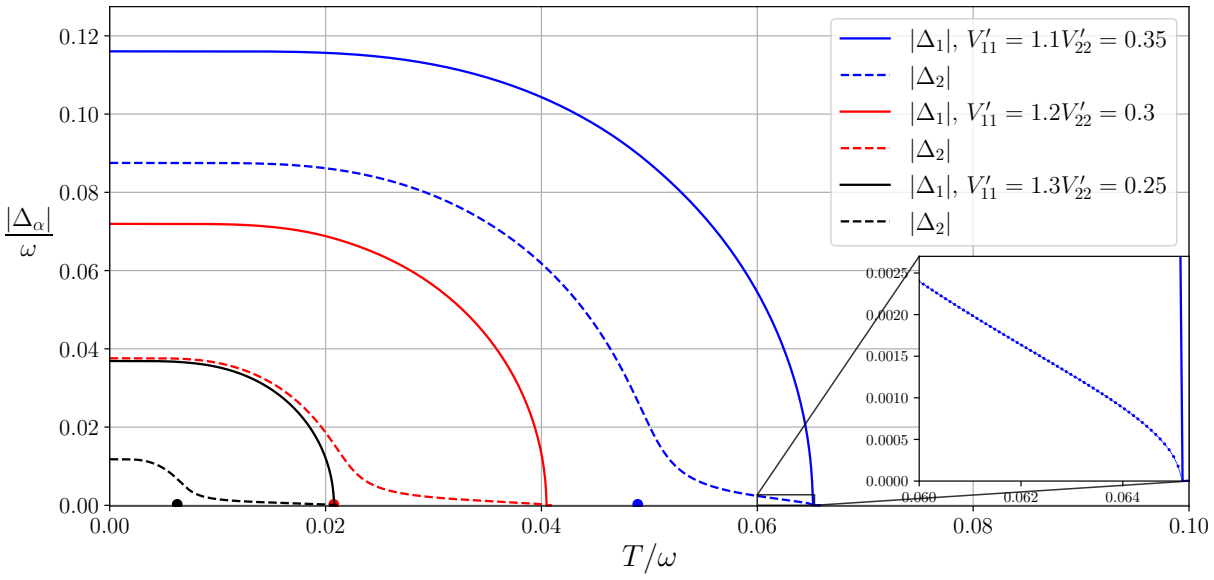

Figure 4.2: Reproduction of Suhl's qualitative diagram showing how the smaller gap does not go to zero at the lower critical temperature (dots) when $V_{12} \neq 0$. The inset shows the critical T-behavior of the second largest gap. Differently colored lines have different intraband potentials, but the dimensionless interband potential $V'_{12} = 10^{-3}$ and $N_1 = N_2$ for all lines. The calculated phase difference was $\theta_{12} = 0$.

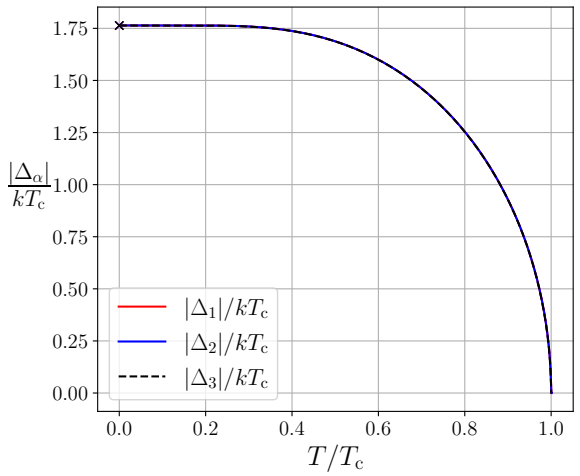

(a) The three calculated gap amplitudes, all overlapping. The two interacting gaps are slightly higher than gap 3, but it is not visible in the figure. Analytical solutions at zero temperature and no coupling are shown as a cross.

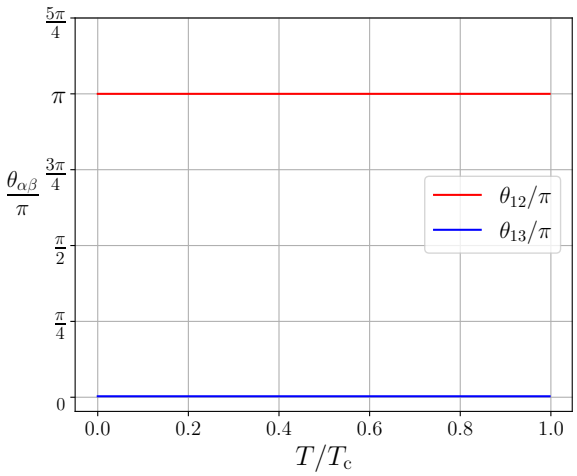

(b) The calculated phase difference between gap 1 and 2 is π to keep yielding a minimum in the free energy.

Figure 4.3: A first calculation using $N = 3$ bands. All $\omega_\alpha = \omega$, $N_\alpha = \text{const}$ and a repulsive interband interaction $V'_{12} = -10^{-5}$ between band 1 and two, much weaker than the intraband interactions, $V'_{\alpha\alpha} = 0.2$. This is at a minimum of the free energy with respect to gap amplitudes and phase differences.

interaction is switched. An example of this is shown in Fig. 4.3 for $V_{12} = -10^{-5}$, which makes $g_{12} > 0$. Making V_{12} attractive makes $\theta_{12} = 0$ because $g_{12} < 0$ in that case. Similar tests show that, in isolation, the other phase differences respond correctly to the sign of their corresponding interband potential.

We now turn on frustration in the problem. To get TRSB, we must turn on all the interband potentials, as explained in section 3.3.1. Using Eq. (3.38), we see that one way to have the signs of $g_{\alpha\beta}$ be positive is to have all the interband potentials weakly repulsive, as Stanev and Tešanović did [26]. We begin with all $V'_{\alpha\alpha} = 0.2$ and all $V'_{\alpha\beta} = -10^{-5}$ with the same densities of states at the Fermi surface for all the bands. As anticipated in [25], the 120° three-armed star emerges, again in analogy with the three antiferromagnetically coupled Heisenberg spins in section 2.4.1 since all gaps and bands are identical in terms of the microscopic parameters. The system nonetheless chooses to spread the gaps out in the complex plane with different phases, but again, with equal phase differences up to a sign. Including a separate figure for the temperature dependence in this case is not necessary because the gaps are essentially the same as in Fig. 4.3, except that $\theta_{12} = 4\pi/3, \theta_{13} = 2\pi/3$ for all T, breaking time-reversal symmetry until the gaps disappear at T_c. We use the word "essentially" because the gap amplitudes are shifted slightly upwards, but by an amount smaller than the symbol sizes in Fig. 4.4.

Stanev and Tešanović report that TRSB is turned off at a temperature $T_{\mathbb{Z}_2} < T_c$ when $V_{23} \neq V_{12} = V_{13}$. Comparison becomes difficult at this point as we find $T_{\mathbb{Z}_2} \approx T_c$ for values of V_{23} near V_{12}. The reason for this discrepancy may be that we have not put $V_{\alpha\alpha} = 0$ like they did, so the gap amplitudes are mostly dominated by the intraband couplings and are not as sensitive to changes in the interband couplings. To illustrate that $V_{\alpha\alpha}$ dominate as well as how we can get $T_{\mathbb{Z}_2}$ much lower than T_c, we can set $V'_{11} = 0.2$, $V'_{22} = 0.19$, and $V'_{33} = 0.18$ while keeping $V'_{\alpha\beta} = -10^{-5}$. This configuration of intraband potentials makes $|\Delta_3|$ become minuscule compared to the other gaps at a temperature far below T_c as is shown in Fig. 4.4. As $|\Delta_3|$ does this, we see in Fig. 4.4a that TRSB is turned off at about $0.5T_c$, demonstrating how we can lower $T_{\mathbb{Z}_2}$ by changing $V_{\alpha\alpha}$. Now, we must emphasize that the only results expected to be exact for this 3D system are the $T = 0$ ones. For higher temperatures, especially those where one gap has begun its

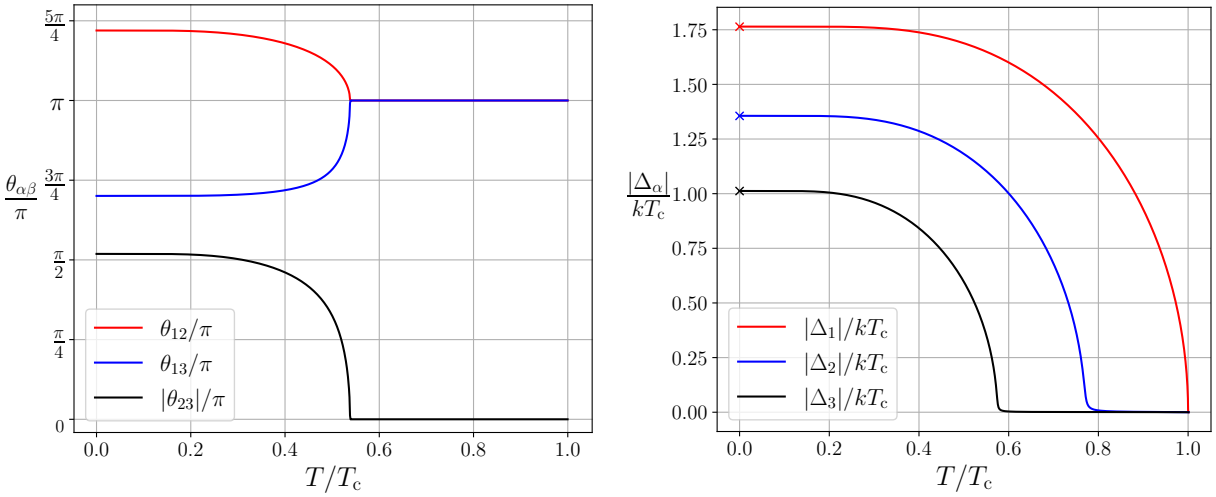

(a) Phase differences **(b)** Gaps

Figure 4.4: $N = 3$ bands where all $\omega_\alpha = \omega$, $N_\alpha = $ const. and with repulsive interband interactions $V'_{\alpha\beta} = -10^{-5}$ between all bands, much weaker than the intraband interactions which were set to $V'_{11} = 0.2$, $V'_{22} = 0.19$, and $V'_{33} = 0.18$. The third gap decreases to a value close to zero after $0.5T_c$ due to its weak intraband interaction, which makes the TRSB disappear since the best way to solve the frustration is to let $\theta_{12} = \theta_{13} = \pi$ when the last gap has almost disappeared.

descent towards zero, effects not present in mean-field theory likely become important [39, 40, 29, 32]. Once again, the gaps do not go all the way to zero near where they would have if they had not been coupled. Instead, they exhibit the same critical behavior near T_c as in the inset in Fig. 4.2. When the third gap is nearly gone (for $T > 0.5T_c$), the system solves the frustration in a non-time-reversal symmetry breaking way, allowing the two cosine factors $g_{12}, g_{13} > g_{23}$ to "win".

4.3 TRSB and tuning of the chemical potential

We have now tested the equation solver against various known cases as well as some new ones, and we have seen some limitations in the model for too large intraband potentials. In this section, we replicate one old result yielding TRSB – now varying a *microscopic* parameter – and show how TRSB can be turned on and off by changing the chemical potential in such a way that it does or does not cross the highest energy band. First, we will vary interband potentials, essentially keeping all the energy bands (2.18) at the same height $\varepsilon_{0,\alpha} = 0$. Afterwards, we will place them at different heights and increase the chemical potential while keeping the other potentials fixed until time-reversal symmetry is broken.

4.3.1 TRSB controlled by interactions

We begin by turning our attention to the phenomenological results from [31] where TRSB was turned on by increasing g_{23} to values beyond 7.5 while keeping $g_{12} = g_{13} = 15$. How can we obtain similar results by varying the microscopic parameters? Let us set all N_α equal and $V'_{\text{inter}} \equiv V'_{12} = V'_{13} = -10^{-5}$ repulsive while we vary V'_{23}, or equivalently, V_{23}. Then the gaps Δ_2 and Δ_3 should be equal in magnitude as the microscopic parameters are all symmetric upon interchange $2 \leftrightarrow 3$ of band indices. With this, we can expect $g_{12} = g_{13}$ since also $V_{12}^{-1} = V_{13}^{-1}$, as can be confirmed by consulting Eq. (3.38). To make the system frustrated and thus have a chance at finding TRSB, we now choose $V_{23} < 0$, making all $g_{\alpha\beta} > 0$. The results at $T = 0$ are shown in Fig. 4.5 where V_{23} is decreased from $V_{\text{inter}}/10$ to about $2.5V_{\text{inter}}$. The phase difference θ_{23} in Fig. 4.5a shows the same non-analytic behavior as in [31] when going from being

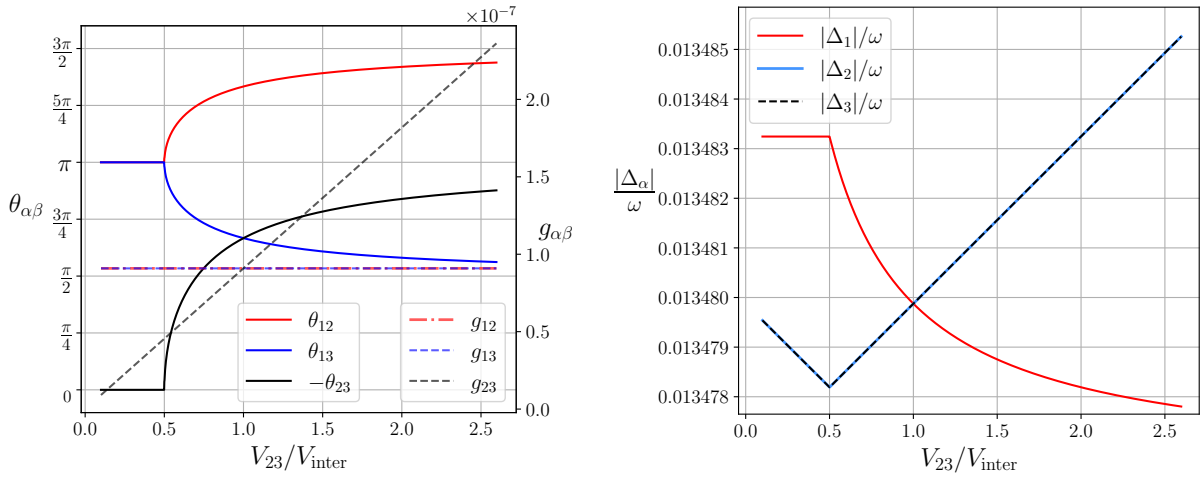

(a) Phase differences and the cosine prefactors $g_{\alpha\beta}$ which are the numbers determining the phase differences. The system transitions from time-reversal symmetric to time-reversal symmetry breaking when θ_{23} non-analytically becomes nonzero after $V_{23}/V_{\text{inter}} = 0.5$.

(b) The gap magnitudes over the same potential interval as in the left figure. The variations are small compared to the gap magnitudes themselves, in line with the fact that $|V_{23}| \ll V_{\alpha\alpha}$. Also here there is non-analytic behavior at the point $V_{23}/V_{\text{inter}} = 0.5$.

Figure 4.5: Zero-temperature demonstration of how TRSB can be controlled by varying one of the interband potentials of a three-band superconductor. All energy cutoffs $\omega_\alpha = \omega$, densities of states $N_\alpha = N$, and the remaining dimensionless interband potentials were kept at $V'_{12} = V'_{13} = -10^{-5} \equiv V'_{\text{inter}}$. The intraband potentials were identical, $V'_{\alpha\alpha} = 0.2$.

constantly 0 to having a kink at the upper threshold of V_{23}/V_{inter} and increasing smoothly towards π after the transition. The onset of TRSB is at the same threshold as that of g_{23}/g illustrated in Fig. 3.1 and in [31], that is, when $V_{23}/V_{\text{inter}} = 0.5$. We see why this is: in the entire range of repulsive potentials V_{23}, the cosine prefactor g_{23} is directly proportional to V_{23}/V_{inter} while the other two remain constant. Therefore, this figure is indeed essentially the same as the one in [32] because $V_{23}/V_{\text{inter}} = g_{23}/g$. We also remark that Fig. 4.5b shows the gap magnitudes varying slightly when the coupling is changed, with non-analytic behavior at the same transition point as the phases. They are once again dominated by the intraband potentials. It is interesting to note that before the onset of TRSB, $|\Delta_1|$ is unaffected by the change of V_{23}, but after the onset when the phases are constrained to change to minimize the free energy, so is $|\Delta_1|$. The onset of TRSB forces all the gaps and phases to change even though the one parameter being changed, V_{23}, involves only band 2 and 3.

These results show that, at least for weakly repulsive interband interactions, engineering the cosine prefactors $g_{\alpha\beta}$ in the free energy to create TRSB is not very difficult at $T = 0$. They depend linearly on the interband potentials in this regime. We also ran zero-temperature calculations decreasing $V'_{12} = V'_{13}$ from -10^{-6} to about -2×10^{-5} while keeping $V'_{23} = -10^{-5}$ and all other theory parameters constant. Here, $g_{12} = g_{13}$ were proportional to the ratio V_{inter}/V_{23}, again allowing easy control of the $g_{\alpha\beta}$'s. We now turn to a slightly more realistic model, serving as a demonstration of how one in principle can go from two bands crossing the Fermi surface in e.g. an iron pnictide compound to three bands and TRSB.

4.3.2 TRSB controlled by tuning μ

In this section, we increase the chemical potential μ from a value below the third band's minimum, $\varepsilon_{0,3}$, until it eventually crosses all three of our parabolic bands from Fig. 2.3a, increasing the density of states N_3 from 0 to a finite value. We will do this with fixed potentials $V_{\alpha\alpha}, V_{\alpha\beta}$ and the same values for $\varepsilon_{0,\alpha}$ as in Fig. 2.3a.

To fix the potentials, we will indicate what the dimensionless potentials must equal to when we reach $\mu_{\max}$. We first parametrize $\mu(t) = t\mu_{\max}$ with $0.6 \leq t \leq 1$, just like in Fig. 2.3a. Since we are studying three-dimensional materials, we assume densities of states of the form

$$N_\alpha(\varepsilon; t, t_\alpha) = A\sqrt{|\varepsilon - \varepsilon_{0,\alpha}|}\Theta(\varepsilon - \varepsilon_{0,\alpha}) = A\sqrt{|\varepsilon - t_\alpha\mu_{\max}|}\Theta(\varepsilon - t_\alpha\mu_{\max}) \tag{4.5}$$

at energy ε and that the bottom of band α is at energy $\varepsilon_{0,\alpha} = t_\alpha\mu_{\max}$. The density of states at the Fermi surface is now

$$N_\alpha(t, t_\alpha) = A\sqrt{\mu_{\max}}\sqrt{|t - t_\alpha|}\Theta(t - t_\alpha), \tag{4.6}$$

where $\Theta(x)$ is the Heaviside step function. This makes it possible to determine the ratios $N_{\alpha\beta}(t, t_\alpha, t_\beta)$ which have to be fed to the equation solver. Whenever either t_α or t_β is larger than t, we set the ratio to zero to avoid dividing by zero. With the naive definition of the density of states ratios, zero division would only have appeared in the gap equations for Δ_3, which must be zero since the momentum shell around the Fermi surface is empty: $F_3 = \emptyset$.

We can now fix the potentials $V_{\alpha\alpha} = f_{\alpha\alpha}V_{11}$ for all α and $V_{\alpha\beta} = f_{\alpha\beta}V_{12}$ for $\beta \neq \alpha$ to find the parametrization for $V'_{\alpha\beta}(t)$. Obviously $f_{11}, f_{12} = 1$, but the other dimensionless factors $f_{\alpha\beta}$ can be chosen at will to adjust the magnitudes of the potentials relative to the two references V_{11} and V_{12}. Inserting this parametrization into the definition of the dimensionless potentials $V'_{\alpha\beta} = V_{\alpha\beta}\sqrt{N_\alpha N_\beta}$ yields

$$V'_{\alpha\beta}(t) = \begin{cases} f_{\alpha\alpha}V'_{11}(t=1)\left(\frac{|t-t_\alpha|}{1-t_1}\right)^{1/2}\Theta(t-t_\alpha) & \text{if } \alpha = \beta \\ f_{\alpha\beta}V'_{12}(t=1)\left(\frac{|t-t_\alpha||t-t_\beta|}{(1-t_1)(1-t_2)}\right)^{1/4}\Theta(t-t_\alpha)\Theta(t-t_\beta) & \text{if } \alpha \neq \beta \end{cases}. \tag{4.7}$$

Choosing $t_1 = 0$, $t_2 = 0.4$, $t_3 = 0.8$, the same values as in Fig. 2.3a, we are now ready to gradually increase t from 0.6, i.e. $\mu(t) < \varepsilon_{0,3}$, to 1, at which point $\mu(t) = \mu_{\max} > \varepsilon_{0,3}$. In Fig. 4.6 we plot the phase differences and gap magnitudes at $T = 0$ for such a calculation with $f_{22} = 1.25$, $f_{33} = 1.75$, and $f_{13} = 6$, $f_{23} = 10$, using $V'_{11}(t = 1) = 0.2$ and $V'_{12}(t = 1) = -10^{-5}$. The latter two definitions also implicitly fix $\mu_{\max}$. The left figure shows that before the Fermi surface crosses the third band, the system chooses the usual $\theta_{12} = \pi$ one has for $N = 2$ and a weakly repulsive interband coupling. When the system becomes a three-band system at $\mu(t) = t_3\mu_{\max} = \varepsilon_{0,3}$, there is almost no frustration, as both g_{13}, g_{23} are negligible due to $|\Delta_3|$'s almost being zero, so the phases take on the same values as in the almost analogous case of Fig. 4.4b after $|\Delta_3|$ has almost disappeared. At a certain point just before $\mu(t) = 0.9\mu_{\max}$, the third and smallest gap reaches a threshold value which, coupled with its large potentials, makes it preferable to solve the now present frustration in a way that breaks time-reversal symmetry. After the threshold is reached, θ_{23} increases rapidly from 0 in the usual order parameter-like manner from before. We note that in contrast to the previous calculations, $|\Delta_3|$ does not display a kink or non-analytic behavior at the threshold value. Due to the large potentials related to gap 2 and 3, the cosine prefactors g_{13}, g_{23} increase quite rapidly compared to the gaps, which is reflected in the phase differences: both θ_{13} and θ_{23} start approaching their target, π whereas θ_{12} is pushed away. The choice of large potentials was of course intentional and done to compensate for the following fact. For all intra- and interband potentials equal, respectively, but otherwise using the same parameters as above, there was no TRSB because the third gap came out several orders of magnitude smaller than gap 1.

The choice of dispersion relations above is likely rather artificial, but the goal was to demonstrate that TRSB could be controlled by changing the densities of states at the Fermi surface through tuning of the chemical potential. This seems firmly established now, having shown the above numerical calculations and the remarks in section 3.3.1. The calculations made here could for instance be extended to model a certain region of the momentum-space with multiple bands crossing it, such as near the Γ point in Figure 5 in [21]. A first step would be to make the bands more closely spaced, perhaps with different curvatures or allowing holes, but we leave this for future considerations.

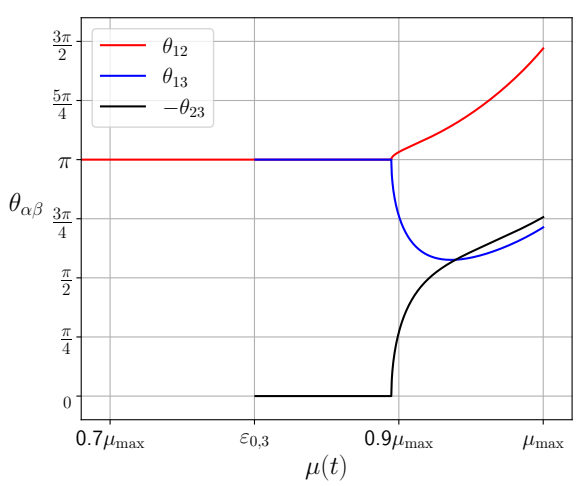

(a) Phase differences obtained from the μ tuning calculation. The same non-analytical behavior of the phase differences when transitioning to a TRSB state near $\mu(t) = 0.9\mu_{\max}$ is present, like in Fig. 4.5a.

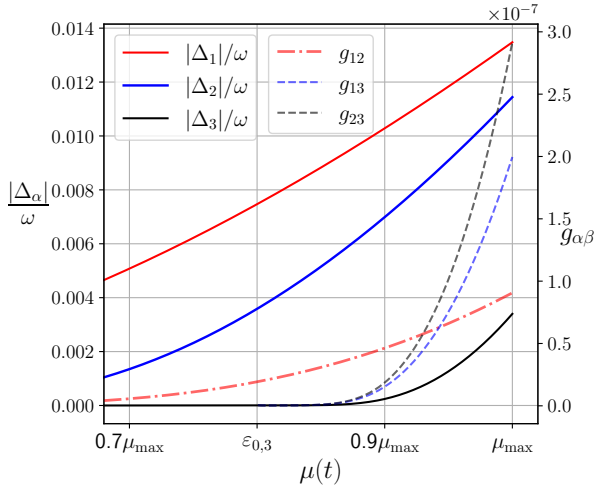

(b) Gap amplitudes obtained from the μ tuning calculation. Unlike Fig. 4.5b, the amplitudes do not have a kink at the threshold μ-value where TRSB is turned on.

Figure 4.6: Result of modeling the tuning of the Fermi surface μ at $T = 0$ to make the superconductor go from $N = 2$ bands to three bands and eventually three bands with TRSB when the phase difference θ_{23} suddenly becomes nonzero. The dispersion relations in Fig. 2.3a were used, and the potentials $V_{33} = 1.75V_{11}, V_{23} = 10V_{12}$ and $V_{22} = 1.25V_{11}, V_{13} = 6V_{12}$ to compensate for the fact that $|\Delta_3|$ is rather small. The reference potentials V_{11}, V_{12} were fixed by setting their dimensionless equivalents to be $V'_{11} = 0.2, V'_{12} = -10^{-5}$ when μ reached $\mu_{\max}$.

Chapter 5

Summary and outlook

In this thesis, we have investigated three-band superconductors at the mean-field level, motivated by the discovery [20, 22] of the class of superconducting materials known as iron pnictides which can exhibit novel superconducting states [24]. The aim of the thesis was to make explicit the microscopic theory behind phase frustration and time-reversal symmetry breaking in these materials and to demonstrate that the multiband character of the iron pnictides is an essential property in producing these qualitatively new effects.

To that end, the thesis began Chapter 2 by extending Bardeen, Cooper, and Schrieffer's microscopic theory of superconductivity [8] to N energy bands crossing the Fermi surface and participating in superconductivity, as suggested by Suhl et al. over 60 years ago [9]. A proper generalization of Bogoliubov's method for diagonalizing the mean-field Hamiltonian without forcing the gap functions to have trivial phases was then applied in Chapter 3, showing how, near the Fermi surface, the quasiparticle excitation spectrum had N gaps given by the modulus of each superconducting gap function.

At this stage, it was possible to identify the origin of the vital phenomenological coefficients $g_{\alpha\beta}$ used elsewhere in Ginzburg-Landau free energy expansions [31, 29, 30] by calculating the free energy based on the diagonalized Hamiltonian. Here, it became clear that whether or not the ground state of the superconductor is phase frustrated is completely determined by the intra- and interband couplings $V_{\alpha\beta}$ because they decide the sign of the matrix inverse $V^{-1}_{\alpha\beta}$ which is multiplied by the positive numbers $|\Delta_\alpha|, |\Delta_\beta|$ to form $g_{\alpha\beta}$. As is explained in the thesis, one cannot obtain time-reversal symmetry breaking from the superconducting gaps without the ground state being phase frustrated. Accordingly, some minimal requirements can be placed on the microscopic parameters $V_{\alpha\beta}$, but this fact is more of a useful tool to check a given set of couplings than it is a recipe for finding couplings conducive to TRSB.

Having established the signs of $g_{\alpha\beta}$ and recognized that they need to be $+++$ or $+--$, we then concerned ourselves with the other crucial component deciding whether the three-band superconductor chooses a TRSB state or not: how is the frustration solved? If two $|g_{\alpha\beta}|$ are too large, they dominate over the last one and lock their corresponding phase differences to the trivial values of 0 or π (see Fig. 3.1). In the intermediate space where the coefficients are comparable or only one is larger than the others, the frustration can be solved in a manner that breaks time-reversal symmetry.

In the numerical section, Chapter 4, we took on the task of finding microscopic parameter values that would give $g_{\alpha\beta}$ conducive to TRSB at $T = 0$. Starting with the known case of equal energy bands with equal intraband couplings and equal and weakly repulsive (to get phase frustration) interband couplings [26–28], we applied the well-known trick of changing only one variable while keeping the others constant and seeing what happened. At this starting point, all $g_{\alpha\beta}$ were expectedly equal and positive, which forced TRSB upon the system. When changing only one of the interband couplings, the corresponding cosine coefficient responded linearly, meaning it could be changed in a controlled manner to tune the system in and out of the TRSB state. In the future, other orders of magnitude for the interband couplings should be explored. Perhaps the same linear response is not found at all scales. We also mention that the $+--$ combination of signs for $g_{\alpha\beta}$ can be studied in our model. With such a sign combination,

Ref. [26] reported that the phase differences would be between $-\pi/2$ and $\pi/2$, i.e. the gaps would be less spread out in terms of angles in the complex plane. Now, changing the microscopic interactions in an iron pnictide sample on demand is likely a difficult enterprise, but these results can at least serve as an example of how the scales of the interband couplings affect whether or not one gets TRSB.

Finally, the slightly more realistic model of three energy bands with different heights was studied. This could serve as a crude approximation of some of the calculated energy bands near the Fermi surface depicted in Figure 5 in [21]. Slight shifts of the Fermi surface there would make fewer bands cross it. We modeled the Fermi surface rising from a low energy below the third band to capture the fact that there was no TRSB until it had reached a certain threshold level rather far above the bottom of the third band. The intra- and interband interactions involving the third band, and to a certain extent the second band, had to be turned up considerably to compensate for the fact that the density of states and hence the gap amplitude in the third band were quite low. In summary, changing the density of states at the Fermi surface of band 3 from 0 to the threshold value yielded a TRSB state at a fixed configuration of couplings, demonstrating how deforming by e.g. an applied voltage or moving the Fermi surface can, in principle, turn TRSB on and off. In more sophisticated calculations with more a more realistic model one could go on to calculate magnetic fields induced by circulating Josephson currents.

The iron pnictides are usually described as having more than three bands [23, 21], so an obvious extension of this work would be to look at the case of $N = 4$ bands or at more realistic dispersion relations. For the latter suggestion, a first step could be to look at more closely spaced energy bands. This would make the densities of states more similar, meaning one could avoid having to boost the potentials in the upper band. Alternatively, bands such as those of Fig. 1 in [24] could be used.

Our zero-temperature mean-field theory results can be expected to be correct due to the Ising-like $\mathbb{Z}_2$ symmetry $\theta_\alpha \to -\theta_\alpha$ of the free energy, F [39, 40]. In principle, fluctuations of various kinds may however become important for finite temperatures, especially near T_c. Phase [29] or gauge [32] fluctuations could for instance affect the temperature at which TRSB is turned off in Fig. 4.5a. We therefore suspect that there lies much work ahead to understand the phase diagram and possible applications of the iron pnictides.

Bibliography

[1] H. K. Onnes, Comm. Phys. Lab. Univ. Leiden **120b, 122b, 124c** (1911).

[2] W. Meissner and R. Ochsenfeld, Die Naturwissenschaften **21**, 787 (1933).

[3] V. L. Ginzburg and L. D. Landau, J. Exp. Theor. Phys. USSR **20**, 1064 (1950).

[4] L. D. Landau, Zh. Eksp. Teor. Fiz. **7**, 19 (1937).

[5] K. Fossheim and A. Sudbø, *Superconductivity*, John Wiley & Sons, Ltd, 2004.

[6] E. Maxwell, Phys. Rev. **78**, 477 (1950).

[7] C. A. Reynolds, B. Serin, W. H. Wright, and L. B. Nesbitt, Phys. Rev. **78**, 487 (1950).

[8] J. Bardeen, L. N. Cooper, and J. R. Schrieffer, Phys. Rev. **108**, 1175 (1957).

[9] H. Suhl, B. T. Matthias, and L. R. Walker, Phys. Rev. Lett. **3**, 552 (1959).

[10] P. Szabó et al., Phys. Rev. Lett. **87**, 137005 (2001).

[11] M. Iavarone et al., Phys. Rev. Lett. **89**, 187002 (2002).

[12] J. Nagamatsu, N. Nakagawa, T. Muranaka, Y. Zenitani, and J. Akimitsu, Nature **410**, 63 (2001).

[13] Y. Tanaka, Journal of the Physical Society of Japan **70**, 2844 (2001).

[14] D. F. Agterberg, E. Demler, and B. Janko, Phys. Rev. B **66**, 214507 (2002).

[15] I. I. Mazin, A. A. Golubov, and A. D. Zaikin, Phys. Rev. Lett. **75**, 2574 (1995).

[16] A. J. Leggett, Progress of Theoretical Physics **36**, 901 (1966).

[17] G. Blumberg et al., Phys. Rev. Lett. **99**, 227002 (2007).

[18] M. Sigrist and K. Ueda, Reviews of Modern Physics **63**, 239 (1991).

[19] M. Sigrist, Physica B: Condensed Matter **280**, 154 (2000).

[20] Y. Kamihara, T. Watanabe, M. Hirano, and H. Hosono, Journal of the American Chemical Society **130**, 3296 (2008).

[21] S. Graser, T. A. Maier, P. J. Hirschfeld, and D. J. Scalapino, New Journal of Physics **11**, 025016 (2009).

[22] M. Rotter, M. Tegel, and D. Johrendt, Physical Review Letters **101** (2008).

[23] K. Nakayama et al., EPL (Europhysics Letters) **85**, 67002 (2009).

[24] V. Grinenko et al., Nature Physics **16**, 789 (2020).

[25] T. K. Ng and N. Nagaosa, EPL (Europhysics Letters) **87**, 17003 (2009).

[26] V. Stanev and Z. Tešanović, Phys. Rev. B **81**, 134522 (2010).

[27] Y. Tanaka and T. Yanagisawa, Solid State Communications **150**, 1980 (2010).

[28] S. Maiti and A. V. Chubukov, Physical Review B **87** (2013).

[29] J. Carlström, J. Garaud, and E. Babaev, Physical Review B **84** (2011).

[30] J. Carlström, J. Garaud, and E. Babaev, Phys. Rev. B **87**, 219904 (2013).

[31] T. A. Bojesen, E. Babaev, and A. Sudbø, Phys. Rev. B **88**, 220511 (2013).

[32] T. A. Bojesen and A. Sudbø, Journal of Superconductivity and Novel Magnetism **28**, 3193 (2015).

[33] C. Kittel, *Introduction to Solid State Physics*, John Wiley & Sons, Inc., 8$^{\text{th}}$ edition, 2004.

[34] J. W. Negele and H. Orland, *Quantum Many-Particle Systems*, Addison-Wesley Publishing Company, 1988.

[35] A. L. Fetter and J. D. Walecka, *Quantum Theory of Many-Particle Systems*, Dover Publications, 2003.

[36] N. N. Bogoliubov, J. Exptl. Theoret. Phys. (U.S.S.R) **34**, 58 (1958).

[37] H. T. Diep, *Frustrated Spin Systems*, World Scientific Publishing Co. Pte. Ltd., 1$^{\text{st}}$ edition, 2004.

[38] M. E. Peskin and D. V. Schroeder, *An Introduction to Quantum Field Theory*, Perseus Books Publishing, L.L.C., 1995.

[39] J. A. Hertz, Phys. Rev. B **14**, 1165 (1976).

[40] A. J. Millis, Phys. Rev. B **48**, 7183 (1993).

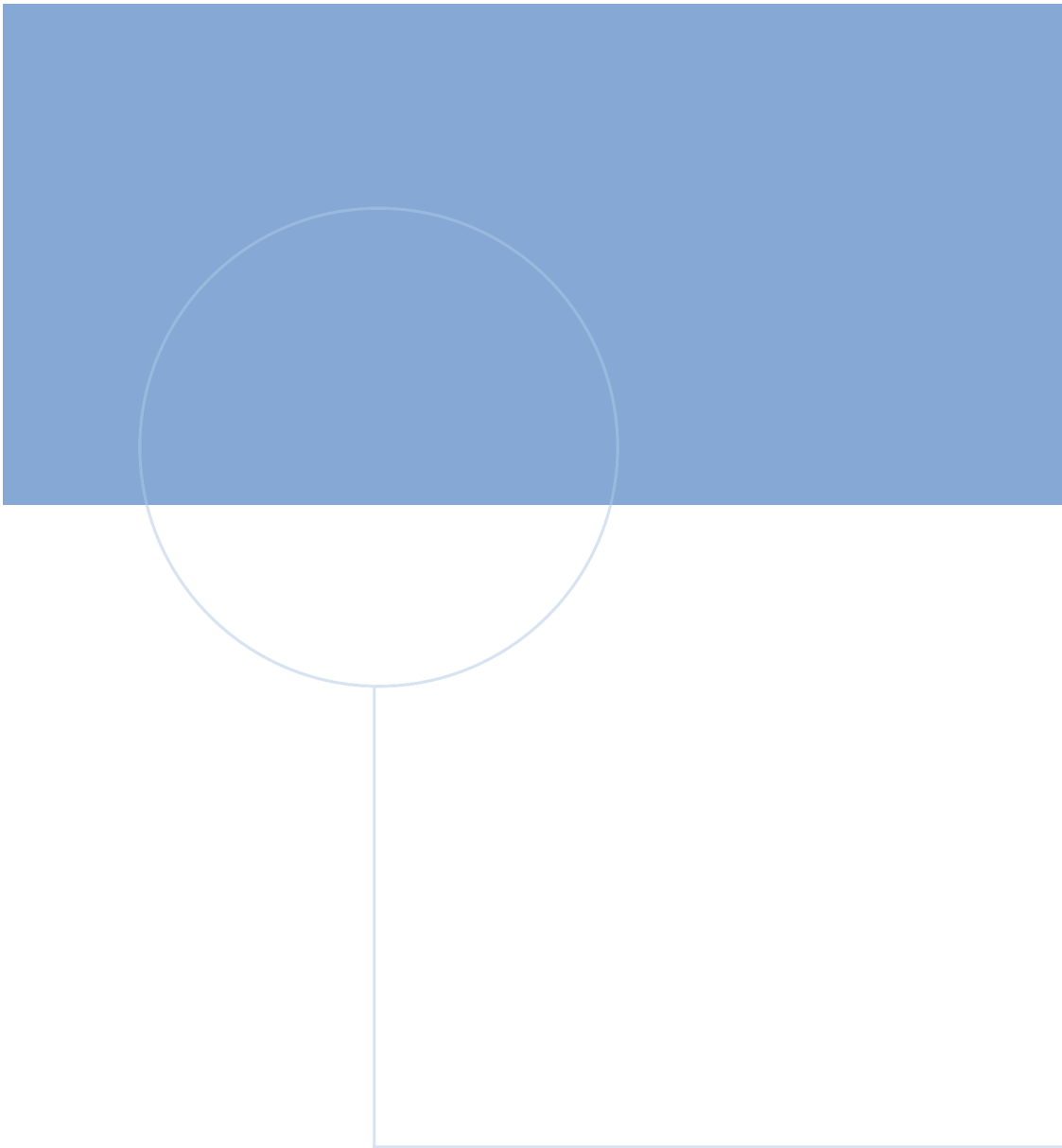

NTNU

Norwegian University of
Science and Technology